Pratt Kerri, A. (Orcid ID: 0000-0003-4707-2290)

Molecular Halogens above the Arctic Snowpack: Emissions, Diurnal Variations, and Recycling Mechanisms

Siyuan Wang[1], Kerri A. Pratt[1,2,*]

[1] Department of Chemistry; [2] Department of Earth and Environmental Sciences, University of Michigan, Ann Arbor, MI, USA

* Corresponding Author: Kerri A. Pratt

Department of Chemistry

University of Michigan, Ann Arbor

930 N. University Ave.

Ann Arbor, MI 48109 USA

prattka@umich.edu

(734) 763-2871

Key Points:

- Heterogeneous uptake of Cl_2 is an important missing sink of Cl_2 and source of BrCl in Arctic models.
- The multiphase reaction of $ClONO_2$ is suggested to play a key role in Arctic snowpack Cl_2 production.
- $Br+BrNO_2/BrONO_2$ may lead to elevated daytime Br_2 under low O_3 conditions, even for "background" NO_x.

This is the author manuscript accepted for publication and has undergone full peer review but has not been through the copyediting, typesetting, pagination and proofreading process, which may lead to differences between this version and the Version of Record. Please cite this article as doi: 10.1002/2017JD027175

Abstract

Elevated levels of reactive bromine and chlorine species in the springtime Arctic boundary layer contribute to ozone depletion and mercury oxidation, as well as reactions with volatile organic compounds. Recent laboratory and field studies have revealed that snowpack photochemistry leads to Br_2 and Cl_2 production, the mechanisms of which remain poorly understood. In this work, we use a photochemical box model, with a simplified snow module, to examine the halogen chemistry occurring during the March 2012 BRomine, Ozone, and Mercury EXperiment (BROMEX) near Utqiaġvik (Barrow), Alaska. Elevated daytime Br_2 levels (e.g., 6-30 ppt at around local noon) reported in previous studies and in this work may be explained by Br + $BrNO_2$/$BrONO_2$ reactions under conditions of depleted O_3 (< ~10 ppb) and background NO_2 (10-100 ppt). Even at low background NO_x levels at Utqiaġvik, $ClONO_2$ is predicted to be important in the production of Cl_2 via heterogeneous reaction with Cl^-. In the late afternoon, photolysis alone cannot explain the rapid decrease of Cl_2 observed in the Arctic boundary layer. Heterogeneous reactions of Cl_2 on aerosol particles and surface snowpack are suggested to play a key role in atmospheric Cl_2 removal and possible BrCl production. Given the importance of the snowpack in the multiphase chemistry of the Arctic boundary layer, future measurements should focus on vertically-resolved measurements of NO_x and reactive halogens, as well as simultaneous particulate and snow halide measurements, to

further evaluate and isolate the halogen production and vertical propagation mechanisms through one-dimensional modeling.

Index Terms

0312 Air/sea constituent fluxes

0322 Constituent sources and sinks

0365 Troposphere: composition and chemistry

0736 Snow

Keywords

Arctic, model, ozone, bromine, chlorine, snowpack

1. Introduction

In the polar boundary layer, reactive halogen chemistry leads to episodic rapid ozone (O_3) depletion [*Barrie et al.*, 1988; *Simpson et al.*, 2007], which affects the oxidative capacity of the atmosphere [*Bloss et al.*, 2010; *Simpson et al.*, 2007], as well as the oxidation and deposition of atmospheric mercury [*Steffen et al.*, 2013]. Tropospheric halogen chemistry has been elaborated in a number of recent reviews [*Abbatt et al.*, 2012; *Simpson et al.*, 2015; *Simpson et al.*, 2007]. Briefly, the major reactions involved in polar halogen cycling are summarized as follows (where X, Y = Cl or Br):

$$X_2 + h\upsilon \rightarrow 2\ X \qquad \text{R1}$$

$$X + O_3 \rightarrow XO + O_2 \quad \text{R2}$$

$$XO + h\upsilon \rightarrow X + O \quad \text{R3}$$

$$XO + HO_2 \rightarrow HOX + O_2 \quad \text{R4}$$

$$HOX + X^-_{(aq)} + H^+_{(aq)} \rightarrow X_2 + H_2O \quad \text{R5}$$

All species are in the gas-phase unless otherwise noted (e.g. aq: aqueous-phase). In addition to forming Br_2 and Cl_2, HOBr and HOCl may undergo cross reactions with Cl^- and Br^- in the snowpack or aerosol forming BrCl (R6):

$$HOX + Y^-_{(aq)} + H^+_{(aq)} \rightarrow XY + H_2O \quad \text{R6}$$

BrCl then undergoes photolysis and re-forms halogen atoms, analogous to R1. In the presence of nitrogen oxides (NO_x: NO + NO_2), XNO_2 and $XONO_2$ can be formed from reactions with reactive halogens:

$$X + NO_2 \rightarrow XNO_2 \quad \text{R7}$$

$$XO + NO_2 \rightarrow XONO_2 \quad \text{R8}$$

$XONO_2$ may also undergo multiphase reactions to form molecular halogens [*Deiber et al.*, 2004]:

$$XONO_2 + X^-_{(aq)} \rightarrow X_2 + NO_3^-{}_{(aq)} \quad \text{R9}$$

$$XONO_2 + Y^-_{(aq)} \rightarrow XY + NO_3^-{}_{(aq)} \quad \text{R10}$$

With the presence of high levels of XO (YO), self-reactions or cross reactions can result in molecular halogen formation, or alternatively, the reformation of halogen atoms [*Simpson et al.*, 2007]:

$$XO + XO \rightarrow X_2 \text{ or } 2X + O_2 \qquad \text{R11}$$

$$XO + YO \rightarrow XY \text{ or } X + Y + O_2 \qquad \text{R12}$$

Elevated levels of molecular halogens, Br_2, BrCl, and Cl_2, have been reported in the polar boundary layer [*Custard et al.*, 2016; *Foster et al.*, 2001; *Liao et al.*, 2012a; *Liao et al.*, 2014; *Neuman et al.*, 2010a; *Spicer et al.*, 2002], yet the production mechanism(s) of molecular halogens remain highly uncertain. Pratt et al [2013] conducted Arctic snow chamber experiments and provided the first direct evidence of photochemical production of Br_2 from the surface snowpack above both tundra and sea ice. In a laboratory study, Wren et al [2013] showed the production of Br_2, BrCl, and Cl_2 from artificial saline snow in the presence of O_3. Most recently, Custard et al [2017] observed the photochemical production of Br_2, BrCl, and Cl_2 in the Arctic snowpack and calculated the snowpack emission fluxes of Cl_2 and Br_2 to the Arctic boundary layer.

A number of previous studies have utilized numerical models to probe reactive halogen chemistry and impacts in the Arctic boundary layer [*Calvert and Lindberg*, 2003; *Cao et al.*, 2014; *Custard et al.*, 2016; *Custard et al.*, 2015; *Evans et al.*, 2003; *Fan and Jacob*, 1992; *Hausmann and Platt*, 1994; *Kaleschke et al.*, 2004; *Le Bras and Platt*, 1995;

Lehrer et al., 2004; *Liao et al.*, 2012a; *Mahajan et al.*, 2010; *Martinez et al.*, 1999; *McConnell et al.*, 1992; *Michalowski et al.*, 2000; *Piot and von Glasow*, 2008; *Piot and von Glasow*, 2010; *Saiz-Lopez et al.*, 2007; *Saiz-Lopez et al.*, 2008; *Sander et al.*, 1997; *Shepson et al.*, 1996; *Spicer et al.*, 2002; *Tackett et al.*, 2007; *Tang and McConnell*, 1996; *Thomas et al.*, 2011; *Thompson et al.*, 2015; *Toyota et al.*, 2014; *Xie et al.*, 2008; *Zeng et al.*, 2006; *Zhao et al.*, 2008]. The potential importance of recycling mechanisms were first highlighted over two decades ago [*Fan and Jacob*, 1992; *McConnell et al.*, 1992]. Michalowski et al [2000] showed that ozone depletion is sensitive to the timescale of HOBr deposition to the snowpack. Lehrer et al. [2004] conducted one-dimensional (1D) modeling, suggesting that heterogeneous chemistry on the sea-ice surface accelerates bromine activation and O_3 depletion. Using a more comprehensive 1D model (MISTRA), Piot and von Glasow [2008] suggested that recycling on the snowpack is important for ODE development. Piot and von Glasow [2010] later investigated the impacts of HCHO, H_2O_2, Cl_2, and HONO on the halogen and ozone chemistry in the polar boundary layer. The coupling of NO_x and halogen chemistry in the Arctic boundary layer has been investigated [*Cao et al.*, 2014; *Custard et al.*, 2015; *Evans et al.*, 2003], suggesting that $BrONO_2$ may greatly affect the halogen-driven O_3 depletion, as well as the NO_x budget, although $BrONO_2$ has not been measured in the Arctic boundary layer. However, the evaluation of these previous models has been limited by few speciated measurements of trace halogen gases. Recent modeling studies have largely been constrained to ambient

measurements, and have explored the bromine speciation as well as the impacts of observed halogens on ozone destruction, oxidative capacity, and the dependency on NO_x [*Custard et al.,* 2016; *Custard et al.,* 2015; *Thompson et al.,* 2015] .

Recent 1D models have incorporated snowpack microphysics and chemistry providing insights into the role of snowpack halogen production and implications on ozone and atmospheric mercury [*Thomas et al.,* 2012; *Thomas et al.,* 2011; *Toyota et al.,* 2014]. It has been shown that snow photochemistry plays an important role in the Arctic [*Grannas et al.,* 2007]. The presence of a disordered interface on snow grain surfaces serves as a reactor for aqueous-phase reactions [*Bartels-Rausch et al.,* 2014]. Previous snowpack atmosphere modeling studies have parameterized snow microphysics and examined the sensitivity of multiphase chemistry to these parameters [*Thomas et al.,* 2011; *Toyota et al.,* 2014]. However, our current understanding and approaches to describe the snowpack have limitations in atmospheric models due to a limited experimental understanding of the nature of the reaction medium [*Bartels-Rausch et al.,* 2014; *Domine et al.,* 2013]. However, given the important role of snow-air interactions in polar atmospheric chemistry [*Dominé and Shepson,* 2002], there is a need to evaluate models with atmospheric chemistry field data, while simultaneously advancing fundamental knowledge of snowpack microphysics.

In the present work, we examine the atmospheric boundary layer measurements of reactive halogen gases conducted during the March 2012 BRomine, Ozone, and Mercury

EXperiment (BROMEX) near Utqiaġvik (formerly known as Barrow), Alaska [*Nghiem et al.*, 2013]. A zero-dimensional multiphase photochemical box model was utilized to explore the coupled gas-phase and heterogeneous chemistry on atmospheric particles and the snow surface. Given uncertainties associated with our limited knowledge of the snow grain surface [*Domine et al.*, 2013], we present here a simplified snow surface model, in place of a more detailed 1-D snowpack model [*Thomas et al.*, 2011; *Toyota et al.*, 2014]. We focus on investigating snowpack molecular halogen emissions and heterogeneous chemistry on boundary layer reactive halogen chemistry. The model outputs, including estimated molecular halogen fluxes, are compared to measurements of reactive halogen species and previous modeling efforts.

2. Ambient Measurements

Solar radiation, wind speed and direction, temperature, pressure, methane (CH_4), ethane (C_2H_6), propape (C_3H_8), temperature, pressure, total O_3 column, and aerosol size distribution measurements were conducted at the NOAA Barrow Observatory (http://www.esrl.noaa.gov/gmd/obop/brw/). Table S1 summarizes ambient measurements in this study. Figure S1 shows the wind speed and direction data for two case study days: 15 and 24 March 2012. Aerosol size distributions (10-800 nm, mobility diameter) were measured using a TROPOS-type mobility particle size spectrometer (MPSS) [*Wiedensohler et al.*, 2012]. Figure S2 shows the average measured aerosol size distributions. Submicron aerosol particles were collected daily on filters at the NOAA

Observatory, and then the aerosol inorganic ion composition was measured using ion chromatography [*Quinn et al.*, 2002]. Vertical profiles (from ~0.2 to ~3 km) of temperature and potential temperature were measured using a Best Air Turbulence (BAT) probe [*Garman et al.*, 2006] on the Purdue Airborne Laboratory for Atmospheric Research (ALAR) during flights originating from the Utqiaġvik airport on 15 and 24 March 2012. See the supplementary information, and Figure S3 for additional details about the vertical atmospheric structure during the model case study time periods, described below.

In situ Br_2, BrO, HOBr, Cl_2, and ClO mole ratios were measured using a chemical ionization mass spectrometer (CIMS) from March 3-28, 2012, at a coastal tundra site (71° 16.500 N, 156° 38.426 W) near Utqiaġvik, AK [*Custard et al.*, 2016; *Peterson et al.*, 2015], located 5.1 km across flat tundra to the southeast of the NOAA Barrow Observatory. Detailed description of the CIMS instrument can be found elsewhere [*Custard et al.*, 2016; *Liao et al.*, 2011]. Sampling and analysis details are explained here and in supplemental section S1. CIMS sampling occurred 1 m above the snowpack with a specially designed inlet to minimize losses of trace gases [*Liao et al.*, 2011]. The inlet included a custom three-way valve for calibration and background measurements [*Liao et al.*, 2011]. Hydrated I^- clusters ($I\cdot(H_2O)_n^-$) were used as the reagent ion to measure and quantify Br_2 (masses 287($I^{79}Br^{81}Br^-$) and 289($I^{81}Br^{81}Br^-$), Cl_2 (masses 197($I^{35}Cl^{37}Cl^-$) and 199($I^{37}Cl^{37}Cl^-$)), BrO (masses 222($I^{79}BrO^-$) and 224($I^{81}BrO^-$), ClO (masses 178($I^{35}ClO^-$)

and 180($I^{37}ClO^-$), and HOBr (masses 223 ($IH^{79}BrO^-$) and 225 ($IH^{81}BrO^-$)), with isotopic ratios used for verification of ion identities [*Custard et al.*, 2016; *Liao et al.*, 2012a].

CIMS background measurements were performed every 15 min by passing the air flow through a glass wool scrubber, which has been shown to remove halogen species at >95% efficiency [*Liao et al.*, 2012b; *Neuman et al.*, 2010b]. Br_2 and Cl_2 calibrations were performed every 2 h by adding Br_2 and Cl_2, from separate permeation sources, each in 21 mL min^{-1} N_2, to the air flow; permeation rates were determined by the optical absorption method described by *Liao et al.* [2011]. BrO, ClO, and HOBr were calibrated using relative sensitivity factors of 0.47 (±25%) [*Liao et al.*, 2011], 0.26 (±42%) [*Custard et al.*, 2016], and 0.5 (±25%) [*Liao et al.*, 2012b], respectively. For a measurement cycle of 10.6 s, masses 287(Br_2), 197(Cl_2), 224(BrO), 178(ClO), and 225(HOBr) were monitored for 0.5 s each, with a 5% duty cycle for each mass. For the model case study days of 15 and 24 March 2012, the CIMS 3σ limits of detections (LODs) calculated were 3.6, 1.5, 1.8, 2.8, and 2.5 ppt for Br_2, Cl_2, BrO, ClO, and HOBr, respectively, on average, for a 2.8 s integration period (corresponding to 1 min of CIMS measurements). Since the variance in the background is likely due to counting statistics [*Liao et al.*, 2011], the LODs for 1 h averaging are estimated to be 0.5, 0.2, 0.2, 0.4, and 0.3 ppt for Br_2, Cl_2, BrO, ClO, and HOBr, respectively. Considering calibration uncertainties and signal variations, the uncertainties in the reported 1 h average Br_2, Cl_2, BrO, ClO, and HOBr mole ratios were calculated to be (15%+0.5 ppt), (28% +0.2 ppt), (29% +0.2 ppt), (56%

+0.4 ppt), and (35% +0.3 ppt), respectively. For the reported 30 min Cl_2 data, the average LOD and uncertainty were calculated to be 0.3 ppt and (26% + 0.3 ppt), respectively. All times are Alaska Standard Time (AKST, UTC-9) in this work, unless otherwise noted. O_3 was measured using a 2B Technologies model 205 dual-beam O_3 monitor, which sampled from the high-flow CIMS inlet.

3. Model Description

To examine the multiphase halogen chemistry occurring near Utqiaġvik, AK on 15 and 24 March 2012, a zero-dimensional (0-D) model was developed using the model framework previously described by Wang et al [2015]. Additional details and a schematic diagram of the model structure are given in the supplemental information and Figure S4. The 0-D model solves a set of ordinary differential equations describing the temporal evolution of species of interest:

$$\frac{dC_g}{dt} = P - L + E - D - \sum^{i:p,s} k_{t,i}(C_g LWC_i - \frac{C_{a,i}}{HRT}) \qquad \text{Eq.1}$$

where i denotes either particle (p) or snow (s). C_g and $C_{a,i}$ are the gas- and aqueous-phase concentrations of a given species (both in molec cm^{-3} air), P and L are the chemical production and loss terms (both in molec cm^{-3} s^{-1}), and E and D are the emission and deposition terms (both in molec cm^{-3} s^{-1}). The last term in Eq.1 describes the phase-transfer of soluble species to both particle liquid water and a surface snow liquid-like

layer. $k_{t,i}$ (s^{-1}) is the phase-transfer coefficient (see details in Sections S2.4 and S2.5), LWC_i (volume fraction) is the liquid water content on particles or snow surface (see details in Sections S2.4 and S2.5), and H (M atm^{-1}) is the Henry's law constant from Sander [2015]. i denotes either particle (p) or snow (s). This system of ordinary differential equations was solved by using Igor Pro 6 (Wavemetrics, Lake Oswego, OR, USA). Key modeling aspects (air-snow interactions and snowpack emissions) are elaborated in the following sections.

The model includes (i) gas-phase chemistry Thompson et al [2015] [*Atkinson et al.*, 2006; *Burkholder et al.*, 2015; *Orlando and Burkholder*, 2000]; (ii) photolysis reactions, with j-values calculated using the NCAR Tropospheric Ultraviolet and Visible Radiation Model (https://www2.acom.ucar.edu/modeling/tropospheric-ultraviolet-and-visible-tuv-radiation-model); (iii) heterogeneous reactions on both aerosol particles and snow grains in the surface snow layer [*Ammann et al.*, 2013; *Deiber et al.*, 2004; *Hu et al.*, 1995; *Sander and Bottenheim*, 2012]; (iv) aqueous-phase reactions in both deliquescent particles and a liquid-like layer on snow grains in the surface snow layer, following Thomas et al [2011] and Toyota et al [*Beckwith et al.*, 1996; *Liu and Margerum*, 2001; *Oum et al.*, 1998; 2014; *Wang and Margerum*, 1994]; (v) dry deposition of trace gases [*Wesely*, 1989]; and (vi) prescribed snowpack trace gas emissions. Gas-phase, photolysis, heterogeneous, and aqueous-phase reactions involving chlorine and bromine species are summarized in Tables S2-S5. Initial concentrations of key species are given in Table S6.

Dry deposition velocities are given in Table S7, and snowpack emissions are elaborated in Tables S8 and S9. Time-resolved ambient temperature and pressure measured at the NOAA Barrow Observatory were used as model inputs. Model spin-up time was 48 h.

3.1. Surface Snowpack Module

Due to the challenges and difficulties in the current state of snow models [*Domine et al.*, 2013], we do not attempt to model the snow-air exchange explicitly. Rather, the influence of snowpack is simplified as the surface layer (top 3 mm) of the snowpack, with the following governing reactions: (i) phase-transfer and subsequent aqueous reactions in a liquid-like layer (LLL) on the surface of snow grain; and (ii) heterogeneous reactions on the surface of snow grains. Mass transport limitation in the snowpack interstitial air is included based on *Pöschl et al.* [2007]. To partially account for the lack of vertical scale in this 0-D model, a scaling factor is applied so that the snowpack is only in partial contact with the overlying ambient air (see Section S3). In addition to the aqueous-phase and heterogeneous chemistry for the surface snow layer, we also include radiation-dependent snowpack emission fluxes for key species (see Section 3.2 for more details), to represent the physical and chemical processes occurring beyond the surface snow layer. The surface snow thickness is defined as 3 mm, i.e. only a few layers of snow grains. This is supported by the modeled snowpack vertical distributions [*Toyota et al.*, 2014], wherein key species (such as O_3, Br_2, $Cl^-_{(aq)}$, $Br^-_{(aq)}$) and parameters (such as pH) do not show dramatic differences in the surface layer of snow (within a few mm of the

surface). The importance of surface snow layer in the air-snow interactions is highlighted in previous studies [*Erbland et al.*, 2013; *Frey et al.*, 2009; *Savarino et al.*, 2013; *Traversi et al.*, 2014].

Snow grains in the model are uniformly set to 0.5 mm in radius (r_s, more details given in SI text S2.6), following Toyota et al [2014] (0.3 mm) and Thomas et al [2011] (1 mm). These microphysical parameters are generally consistent with snow measurements in Utqiaġvik, AK [*Domine et al.,* 2012]. Snow density is assumed to be 0.3 g cm^{-3} based on measurements in Utqiaġvik in March-April 2009 showing approximately 0.2-0.3 g cm^{-3} at the snow surface [*Domine et al.*, 2012]. The corresponding specific surface area of the surface snow layer is then calculated to be 133 cm^2 g^{-1}, comparable to measurements (45-224 cm^2 g^{-1}) during March-April 2009 at Utqiaġvik [*Domine et al.*, 2012]. The volume-based snow grain surface area density (μm^2 cm^{-3}) is used to calculate the heterogeneous reaction rates on snow grains. Liquid-like layer thickness typically ranges from ~0.3 nm (roughly the diameter of a water molecule) to 100 nm, depending on temperature [*Bartels-Rausch et al.*, 2014]. In this work we chose 10 nm, the same value as used in a previous snowpack model [*Thomas et al.*, 2011], since the temperature measured at 10 m above the surface (240-250 K) in this work is comparable to that in Thomas et al (240-260 K). Based on the LLL thickness, snow grain size, and snow density, the LLL volume fraction is then calculated to be 4×10^{-5}, comparable to that used by Toyota et al [2014] (1.1×10^{-5}) in a previous snow modeling study.

3.2. Radiation-Dependent Snowpack Emissions

Radiation-dependent snowpack emission rates of NO_2, H_2O_2, HONO, Cl_2, and Br_2 are included in the model to reflect photochemical production of these compounds based on previous studies [*Custard et al.*, 2017; *France et al.*, 2012; *Grannas et al.*, 2007; *Pratt et al.*, 2013]. Emission rates of NO_x, H_2O_2, and HONO (Table S9) are scaled with photolysis frequencies, i.e. j-NO_2, j-H_2O_2, and j-HONO, respectively. Emission rates of Cl_2 and Br_2 are parameterized in two ways: (i) JScale: emission rates (F_{X2}) are scaled linearly with j-values (i.e. $F_{X2} \propto j_{X2}$, where $X_2 = Cl_2$ or Br_2); (ii) SS: emission rates are scaled with steady-state (SS) removal (i.e. $F_{X2} \propto j_{X2} \cdot [X_2]$). The SS parameterization is based on the steady-state assumption, that the snowpack emission rates of Br_2 and Cl_2 are balanced by their photolysis, due to the short daytime photolysis lifetimes of Br_2 and Cl_2 in the Arctic (tens of seconds and tens of minutes, respectively, for March 2009 in Utqiaġvik; Thompson et al., 2015). In each parameterization, further modifications were made to best fit measurements (i.e. JScale_Mod and SS_Mod refer to modifications made based on JScale and SS parameterizations, respectively) to examine temporal trends in fit emission rates.

4. Results and Discussion

4.1. 15 and 24 March: Case Studies

15 and 24 March 2012 were selected for case studies of halogen chemistry near Utqiaġvik, AK based on comprehensive data coverage and elevated reactive bromine and chlorine levels. Cl_2, ClO, BrO, and O_3 data for the BROMEX measurements can be found in Custard et al [2016] and Peterson et al [2015]; a full time series for Br_2 is shown in Figure S5. The measured O_3, Cl_2, ClO, Br_2, BrO, HOBr, and solar radiation for the case study days are shown in Figure 1. 15 March 2012 featured elevated daytime reactive bromine (Br_2, BrO, and HOBr), while reactive chlorine species (Cl_2 and ClO) were relatively low. In contrast, 24 March was a high reactive chlorine day but reactive bromine species were in lower abundance. This allows near isolation of bromine and chlorine chemistry for investigation. Wind speed and direction are shown in Figure S1. Wind at 10 m above the snowpack surface on 15 March was from northeast over snow-covered ice on the Beaufort Sea and traveling at 4-6 m s^{-1}; wind on 24 March (6-8 m s^{-1}) was from the northeast (Beaufort Sea), passing over snow-covered sea ice and a nearby lead [*Moore et al.*, 2014]. Solar radiation on 15 March (maximum: 256 W m^2) was 15% weaker than that on 24 March (maximum: 300 W m^2). O_3 rose from ~1 ppb during the night of 14 March to 12 ppb on the morning on 15 March, followed by depletion to near zero in ~5 h, with subsequent recovery starting at 20:00. On 24 March, O_3 remained at ~33 ppb from midnight to 16:00, then decreased to ~19 ppb between 16:00 and 22:00 and then recovered back to ~34 ppb. Background O_3 levels on 24 March are attributed to

open lead-induced convective mixing bringing O_3 to the surface from above [*Moore et al.*, 2014].

Observed Cl_2 on both 15 and 24 March followed a consistent diurnal pattern (Figure 1), as in previous Utqiaġvik studies [*Custard et al.*, 2016; *Liao et al.*, 2014]. Cl_2 increased at sunrise, implying photochemical production. During the daytime, Cl_2 showed a double-peaked feature, one in the morning and the other in the late afternoon, followed by a decrease to near zero in the early evening with Cl_2 again reaching near zero at night, implying a removal mechanism of Cl_2 in the late afternoon. Chlorine levels were low on 15 March, peaking at 8 ppt in the early morning and 7 ppt in the late afternoon. ClO was consistently below 0.5 ppt. In contrast, 24 March featured elevated Cl_2 and ClO levels, peaking at 20 ppt and 12 ppt, respectively, during daytime [*Custard et al.*, 2016]. During this period, ClO production was previously simulated by constraining Cl_2 levels, suggesting that Cl_2 is the primary source of Cl atoms for ClO formation [*Custard et al.*, 2016].

Reactive bromine levels were relatively low on 24 March compared to 15 March. On 24 March, Br_2 remained at ~20 ppt at night, and decreased rapidly to near zero following sunrise. Daytime BrO and HOBr levels on 24 March reached 20 and 9 ppt, respectively. In contrast, reactive bromine levels were elevated on 15 March: Br_2 maintained between 34 and 53 ppt at night, decreasing at sunrise, followed by sharp increases of BrO (up to 30 ppt) and HOBr (up to 20 ppt) before local noon. The minimum

daytime Br_2 level on 15 March was 9 ppt. The noontime photolysis lifetime of Br_2 on 15 March was 34 s (based on TUV calculated j_{Br2}, see Table S3), which is comparable to the minimum photolysis lifetime (23 s) on 25 March 2009 OASIS campaign near Utqiaġvik, AK [*Thompson et al.*, 2015]. Previously, Neuman et al [2010a] showed the conversion of HOBr to Br_2 with a long sampling line. However, the inlet has been re-designed to significantly minimize residence time (~0.07 s in this study) and wall interactions [*Liao et al.*, 2011]. Despite this, Buys et al [2013] suggested that 20% of Br_2 measured in Antarctica could be from HOBr conversion. Since we now know that Br_2 is photochemically produced from the surface snowpack [*Custard et al.*, 2017; *Pratt et al.*, 2013], we suggest the high daytime Br_2 levels on 15 March are due to strong production and recycling mechanisms, the potential for which is explored in Section 4.3.

4.2. A Missing Sink of Cl_2 in Models

Photolysis is a major sink of Cl_2, with the daytime maximum photolysis corresponding to a lifetime on the order of ~10 min (Table S3). Figure 2 shows the photolysis loss rate ($-[Cl_2]\times j_{Cl2}$) compared to the rate of change in the measured Cl_2 ($d[Cl_2]/dt$), which represents the net result of production and removal in the late afternoon. On both 15 and 24 March, the photolysis loss rate was smaller than the net concentration change rate, implying that photolysis alone is not capable of explaining the rapid depletion of Cl_2 in the late afternoon, consistent with previous results in March 2009 near Utqiaġvik [*Liao et al.*, 2014]. The vertical transport time scale can be used to examine if

the Cl_2 change in the afternoon is due to vertical mixing ($\tau_{\text{vertical transport}} = z^2 / (2K)$ [*Jacob*, 2000], where z is the effective mixing layer height and K is the eddy diffusivity). Assuming a 10 m effective mixing layer height for Cl_2 (Section 4.7) and average K of 95 $cm^2\ s^{-1}$ in the Arctic [*Guimbaud et al.*, 2002], $\tau_{\text{vertical transport}}$ is estimated to be 1.5 h. In the late afternoon (19:00-21:00) $\tau_{\text{vertical transport}}$ is likely even longer due to the weaker turbulent diffusivity and longer photolysis lifetime of Cl_2. The observed Cl_2 lifetime in the late afternoon is 0.6 h and 0.7 h for 15 and 24 March, respectively, much shorter than the characteristic time for vertical transport, implying the rapid depletion of Cl_2 in the late afternoon cannot be explained by vertical mixing alone. Liao et al [2014] reported rapid decrease of Cl_2 in the late afternoon in the campaign average in the same location during spring 2009, implying this common phenomenon is unlikely due to advection. While chlorine chemistry has been included in numerical models [*Custard et al.*, 2016; *Liao et al.*, 2014; *Piot and von Glasow*, 2010; *Thompson et al.*, 2015], the only Cl_2 removal mechanisms included were photolysis and dry deposition. As shown in Figure 2, the Cl_2 dry deposition velocity must be increased by a factor of 50 to explain the rapid decrease of observed Cl_2 in the late afternoon. This suggests that a Cl_2 removal mechanism is missing.

Hu et al [1995] conducted laboratory experiments and suggested that Cl_2 may undergo heterogeneous reactions with bromide to form BrCl, which could react further to produce Br_2:

$$Cl_2 + Br^-_{(aq)} \leftrightarrow BrCl + Cl^-_{(aq)} \quad \text{R13}$$

$$BrCl + Br^-_{(aq)} \leftrightarrow Br_2 + Cl^-_{(aq)} \quad \text{R14}$$

For 15 and 24 March, Figure 2 shows the reaction rate corresponding to this reaction, $k_{het} \times [Cl_2]_{meas}$, where k_{het} is the heterogeneous reaction rate coefficient on aerosols calculated using Eq.S1, and $[Cl_2]_{meas}$ is the measured Cl_2 concentration. The Cl_2 reactive uptake coefficient for aqueous droplets at 263-293 K has been reported up to 0.16, which increases with decreasing temperature [*Hu et al.*, 1995]. Therefore, a reactive uptake coefficient of 0.16 was used to calculated k_{het}; this calculation represents the upper limit of the measurement-derived heterogeneous removal of Cl_2 on aerosols. The Cl_2 loss rate due to this reaction is within the Cl_2 measurement uncertainty (Figure 2), suggesting that this reaction may explain the rapid Cl_2 loss in the late afternoon. At the same location in March 2009, BrCl was correlated with the Cl_2 removal rate [*Liao et al.*, 2014], also suggesting BrCl in the Arctic may be a product from heterogeneous reactions involving Cl_2. As discussed in Section 4.8 and shown in Table 2, while Cl_2 reactions on both particles and snow grains contribute to Cl_2 loss, particle-phase reactions are predicted to play a greater role on 24 Mar, when Cl_2 was elevated, further supporting the heterogeneous removal of Cl_2 on particles as a significant contributor to the afternoon loss of Cl_2 that should be considered in models.

4.3. Effects of O_3 and NO_x on the Daytime Br_2 Levels

Previous studies suggested that reactive bromine chemistry may greatly affect the NO_x budget under pristine background Arctic conditions [*Cao et al.*, 2014; *Evans et al.*, 2003; *Shepson et al.*, 1996]. In a recent field study, Custard et al [2015] discussed the impacts of ppb levels of NO_x on Arctic boundary layer bromine chemistry, finding that anthropogenic NO_x may enhance the removal of BrO. Under background conditions (i.e. without direct influence from the town of Utqiaġvik or Prudhoe Bay), NO_x measured near Barrow can reach up to 190 ppt, with an average of 84 ± 159 ppt in March 2009 [*Thompson et al.*, 2015; *Villena et al.*, 2011]. Here we discuss the effects of this low range of NO_x on daytime Br_2 levels.

Br_2 is a major nocturnal bromine reservoir, and its daytime lifetime is typically short (tens of seconds) due to photolysis. The distribution between Br atoms and BrO is largely controlled by O_3 and BrO photolysis (R2 and R3). Due to the rapid reaction of Br with O_3 [*Burkholder et al.*, 2015], Br_x (Br + BrO) is typically primarily BrO. However, when O_3 is depleted (e.g. <5 ppb), Br atoms are expected to exist in relatively high abundance, as shown in Figure 3. For example, assuming BrO to Br conversion is dominated by photolysis (j_{BrO} = 0.03 s^{-1}), the steady-state Br/BrO molar ratio is 0.24 under the condition of 5 ppb O_3 at 273 K and 101.3 kPa. Further reduction of O_3 to 3 ppb leads to an increase of the steady-state Br/BrO molar ratio to 0.40, consistent with previous studies [*Helmig et al.*, 2012; *Platt and Janssen*, 1995].

In the presence of NO_x, Br and BrO can react to form $BrNO_2$ and $BrONO_2$ via R8 and R9. Orlando and Burkholder [2000] reported rapid gas-phase reactions between Br atoms and $BrNO_2$ and $BrONO_2$ to form Br_2:

$$Br + BrNO_2 \rightarrow Br_2 + NO_2 \qquad R15$$

$$Br + BrONO_2 \rightarrow Br_2 + NO_3 \qquad R16$$

When O_3 is above ~10 ppb, these two reactions can be ignored due to the low abundance of Br atoms. However, when O_3 is depleted, these two reactions may play a substantial role in Br_2 production. Figure 3 shows the calculated noontime Br_2 / BrO and Br / BrO molar ratios under varying O_3 and NO_2 levels. The Br / BrO ratio increases dramatically with decreasing O_3, especially at O_3 < 10 ppb. With increasing NO_2 levels, the Br_2 / BrO ratio increases significantly due to the increased importance of Br_2 production from Br + $BrNO_2$/$BrONO_2$ reactions. Notably, when O_3 is depleted and NO_x is greater than 100 ppt, the noontime Br_2 / BrO ratio can reach 1 or even greater.

Elevated daytime Br_2 levels were frequently observed in Utqiaġvik during March 2012 BROMEX (Figure S5). From 3-28 March 2012, there were 15 days of Br_2 and O_3 measurements when the air did not come from town. Daytime minimum Br_2 remained above 6 ppt during nine out of these 15 clean days (Figure S5). O_3 was below 10 ppb during four out of these nine clean days with high daytime Br_2, consistent with the prediction from Figure 3. On the 15 March case study day, O_3 was depleted and around

zero for most of the daytime (6:00-20:00 AKST Figure 1). Br_2 maintained above 9 ppt, with an average Br_2 / BrO ratio of 2.0 ± 0.9 (Figure 1). In contrast, daytime average Br_2 / BrO was only 0.1 ± 0.9 on 24 March, when O_3 was not depleted. Therefore, the high daytime Br_2 on 15 March can be explained by the recycling involving bromine atoms and NO_x through $BrNO_2$ and $BrONO_2$ (R15 and R16). This scenario is also consistent with elevated Br_2 reported near Utqiaġvik on O_3-depleted days during the March 2009 OASIS campaign [*Liao et al.*, 2012a] when NO_2 data (10-53 ppt, noontime average) [*Thompson et al.*, 2015] were also available (Figure 3).

4.4. HOX vs $XONO_2$ Formation

Both HOX (HOCl and HOBr) and $XONO_2$ ($ClONO_2$ and $BrONO_2$) are important reactive halogen reservoirs and oxidants with respect to X^-. The relative abundance of HO_2 and NO_2 affects the fate of XO: whether formation of HOX (HOBr and HOCl, R4) or $XONO_2$ ($BrONO_2$ and $ClONO_2$, R9) is favored. Figure 4 shows the branching ratio between the $BrONO_2$ and HOBr production rates ($\frac{P_{BrONO_2}}{P_{HOBr}} = \frac{k_{BrO-NO_2}[NO_2]}{k_{BrO-HO_2}[HO_2]}$), as well as $ClONO_2$ and HOCl production ($\frac{P_{ClONO_2}}{P_{HOCl}} = \frac{k_{ClO-NO_2}[NO_2]}{k_{ClO-HO_2}[HO_2]}$), as a function of NO_2 and HO_2 molar ratios. If the ratio (P_{XONO2}/P_{HOX}) is above 1, formation of $BrONO_2$ and $ClONO_2$ are favored, and conversely, if the ratio is less than 1, then the formation of HOBr and HOCl are favored. Based on measured NO_2 and HO_2 during March 2009 near Utqiaġvik [*Thompson et al.*, 2015], formation of $BrONO_2$ is at least as important as HOBr, even at

NO_2 < 50 ppt (Figure 4). This is consistent with the low NO_x scenario (50-100 ppt) in Custard et al [2015]; in this range, the BrO + NO_2 reaction is a factor of two faster than BrO + HO_2 on average. For $ClONO_2$ vs HOCl, formation of $ClONO_2$ is also favored over HOCl under typical background NO_x conditions near Utqiaġvik. These favorable conditions for $BrONO_2$ formation even at local background NO_x levels further support sustained Br_2 formation (R16) and elevated daytime Br_2 levels (Figure 1). This is consistent with the dual isotopic analysis ($\delta^{15}N$ and $\Delta^{17}O$) of atmospheric nitrate during March 2009 near Utqiaġvik: the observed low $\delta^{15}N$ values, indicative of snowpack NO_x emissions, were systematically associated with multiphase nitrate production from $BrONO_2$, as indicated by high $\Delta^{17}O$ values [*Morin et al.*, 2012]. Laboratory studies have shown that HOCl, HOBr, $ClONO_2$, and $BrONO_2$ may undergo multiphase reactions with halides to form molecular halogens (Cl_2, BrCl, and Br_2) [*Beckwith et al.*, 1996; *Caloz et al.*, 1996; *Deiber et al.*, 2004; *Gebel and Finlayson-Pitts*, 2001; *Liu and Margerum*, 2001; *Timonen et al.*, 1994; *Wang and Margerum*, 1994]; the possible contributions of $ClONO_2$ and $BrONO_2$ to halogen activation are discussed in Section 4.8.

4.5. Snowpack Emissions of Br_2

To examine the influence of snowpack Br_2 emissions on the boundary layer halogen chemistry, we conducted zero-dimensional modeling with prescribed radiation-dependent snowpack emission rates of NO_2, H_2O_2, HONO, Br_2, and Cl_2, as described in Section 3.2. As discussed in Section 4.3, the elevated daytime Br_2 observed on 15 March

requires low O_3 (<5 ppb), as observed during the daytime, and elevated NO_x (>20 ppt), for agreement with the observed levels of BrO and HOBr. Since NO_x was not measured in 2012, two background diurnally-varying NO_x scenarios, S1 and S2, consistent with photochemical NO_x production [*France et al.*, 2012], were tested for 15 March. As shown in Table 1, average daytime NO_x in model scenarios S1 and S2 are set to 9 and 70 ppt, respectively, which are both within the previously measured NO_x range in Utqiaġvik during clean periods [*Villena et al.*, 2011]. In each NO_x scenario, the snowpack Br_2 emission rate is parameterized in three ways, as described in Section 3.2. Figure 5 shows measured and modeled reactive bromine species for 15 March for these two sensitivity studies (NO_x S1 and S2).

In the NO_x S1 scenario, regardless of how the snowpack Br_2 emission is parameterized (Jscale, SS, or SSmod), modeled daytime Br_2 levels are always below 6 ppt, much lower than Br_2 measured by CIMS. Further increases in the Br_2 emission rate do not bring modeled daytime Br_2 to the measured level and also overestimate HOBr and BrO. Modeled daytime O_3 is also higher than measured for these scenarios (Figure 5). In contrast, for the NO_x S2 scenario (average daytime NO_x 70 ppt, modeled), however, modeled O_3 and Br_2 both show improved agreement with measurements. High daytime Br_2 can only be achieved with slightly elevated NO_x (NO_x S2 scenario) and depleted O_3, which is in agreement with our analysis in Section 4.3. As shown in Figure 5, the Jscale Br_2 emission rate (NO_x S2) yields inaccurate trends in BrO and HOBr compared to

measurements. The SS Br_2 rate (NO_x S2) gives improved diurnal patterns for both BrO and HOBr, though the species are slightly overestimated in the afternoon. Br_2 is also overestimated in the afternoon and evening in this scenario. The SSmod Br_2 emission rate (NO_x S2), with reduced Br_2 emission in the afternoon (see the shading in Figure 5) produces the best agreements in O_3, Br_2, BrO and HOBr. Similarly, elevated daytime Br_2 observed on 15 March can only be reproduced in the model with slightly elevated NO_x, which still is within the measured NO_x range of background conditions (84±159 ppt at Utqiaġvik, [*Villena et al.*, 2011]). This is again consistent with the role of $BrONO_2$ in Br_2 formation (Section 4.3 and 4.4). Overall, on both 15 and 24 March, improved agreement was achieved with reduced Br_2 emissions in the afternoon (compared to state-state or j-value-scaled emission parameterizations).

4.6. Snowpack Emissions of Cl_2

In this section we explore the influence of snowpack emissions of Cl_2, as observed by Custard et al [2017], on the boundary layer halogen chemistry. Figure 6 shows the modeling results for 24 March with the snowpack Cl_2 emission rates parameterized in the same three ways as for Br_2 (see Section 3.2): (i) JScale: Cl_2 emission rate scales with J_{Cl2}; (ii) SS: Cl_2 emission rate scales with steady-state production rate; and (iii) SS_mod: modified based on SS. As shown in Figures 6 and S7, the model scenario JScale does not capture the double-peaked feature of Cl_2 (maxima in the early morning and the late afternoon) implying the snowpack Cl_2 emission does not linearly

correlate with solar radiation. The SS Cl_2 emission scenario yields improved agreement in diurnal variations of both Cl_2 and ClO, with Cl_2 overestimated in the late afternoon by 40%. By decreasing the Cl_2 snowpack emission by ~30% in the late afternoon (difference shown as shading in Figure 6), the SS_mod Cl_2 emission scenario reproduces the double-peaked diurnal feature of Cl_2 and ClO. Similar model simulations for 15 March, when minimal chlorine activation was observed (Cl_2 <10 ppt), are shown in Figure S6. The SS Cl_2 emission scenario captures the two-peak Cl_2 phenomena on 15 March. SS_mod, with a small increase in the Cl_2 emission rate (difference shown as shading in Figure S6), also produced improved agreements in both NO_x scenarios, similar to 15 March. Overall, scaling the Cl_2 snowpack emission rate with the steady-state production rate produces the best agreement with measurements, while scaling the Cl_2 rate with j_{Cl2} does not produce the correct diurnal profiles for Cl_2 and ClO. An in-depth study of chlorine activation in the snowpack, as well as the mass exchange between the snowpack and the overlying atmosphere, is needed to understand the driving factors in the snowpack Cl_2 emission.

4.7. Modeled Snowpack Emission Fluxes of Cl_2 and Br_2: Comparison with Measurements

In this section, we compare the snowpack Cl_2 and Br_2 emission fluxes estimated from our model scenarios to measurement-derived fluxes [*Custard et al.*, 2017] and previous modeling studies. In order to compare the model-derived snowpack emission rates herein to previously reported snowpack emission fluxes, the noontime emission

rates are converted into emission fluxes, by multiplying the emission rates by the noontime effective mixing layer heights. Due to the short atmospheric lifetimes of Br_2 and Cl_2, it is unrealistic that Br_2 and Cl_2 will be well-mixed throughout the entire modeled box, which is defined by the boundary layer heights for each simulated day (Section S1). Assuming an average eddy diffusivity value of 95 cm^2 s^{-1} [*Guimbaud et al.*, 2002], the noontime photolysis lifetimes of Cl_2 (10 min) and Br_2 (~33 s) correspond to effective mixing heights of 2.4 m for Cl_2 and 0.5 m for Br_2. Multiphase recycling reactions on particles would provide longer atmospheric lifetimes of Cl_2 and Br_2 and therefore, higher effective mixing heights. Since the 0-D model cannot simulate any vertical dependence, we assume noontime effective mixing heights of 10 m for Cl_2 and 1 m for Br_2 to account for photolysis and some multiphase recycling and to allow for comparison with Custard et al [2017].

Using the estimated 10 m effective mixing height, the maximum simulated total snowpack emission flux of Cl_2 is 2.9×10^8 molec cm^{-2} s^{-1} for 15 March (Figure S7, SS_mod, late afternoon) and 3.2×10^8 molec cm^{-2} s^{-1} for 24 March (Figure 6, SS_mod, early morning). In February 2014 near Utqiaġvik, Cl_2 fluxes above the coastal tundra snow surface were determined by the concentration gradient method to be $0.02\text{-}1.4\times10^9$ molec cm^{-2} s^{-1}, with maximum fluxes occurring around local noon [*Custard et al.*, 2017]. Therefore, the Cl_2 snowpack fluxes estimated in this work are in the range of those calculated through the previous springtime vertical gradient measurements [*Custard et al.*,

2017]. Liao et al [2014] calculated the steady-state Cl_2 production rate in March 2009 to be up to 2.2×10^6 molec cm^{-3} s^{-1}, corresponding to a snowpack Cl_2 flux of 2.2×10^9 molec cm^{-2} s^{-1} into a 10 m layer. However, the 2009 springtime average daily maximum Cl_2 levels were up to 60 ppt [*Liao et al.*, 2014], a factor of 3-6 higher than the Cl_2 levels in this work. Toyota et al [2014] explored chlorine activation using a 1D multiphase model, showing a modeled Cl_2 snowpack flux of less than 10^8 molec cm^{-2} s^{-1} (time varying). However, the modeled Cl_2 never exceeded a few ppt above the snowpack, unlike the March 24, 2012 case study day, and the Toyota et al [2014] simulations represent cleaner conditions than Utqiaġvik, AK. The modeled NO_x in Toyota et al [2014] never exceeded ~50 ppt, while higher NO_x levels have been reported near Utqiaġvik even under background conditions [*Villena et al.*, 2011]. Piot and von Glasow [2010] simulated a snowpack Cl_2 emission flux up to 3×10^{11} molec cm^{-2} s^{-1}; however, this led to unrealistically high ClO (ppb level), for which no measurement data were available at the time for comparison.

Br_2 fluxes above the snow surface were measured to be $0.07\text{-}1.2\times10^9$ molec cm^{-2} s^{-1} near Utqiaġvik in February 2014 [*Custard et al.*, 2017], with maximum fluxes occurring around local noon. Noontime Br_2 emission fluxes estimated in this work are 2.1×10^8 molec cm^{-2} s^{-1} for 15 March (Figure 5) and 3.5×10^6 molec cm^{-2} s^{-1} for 24 March (Figure S6). The Br_2 emission flux on 15 March is comparable with the measurement-derived fluxes from February 2014, when the measured Br_2 measured at 1 m above the

snowpack maintained at 8-12 ppt between 9:30 and 15:46 AKST. This is similar to Br_2 levels on 15 March 2012 (minimum 9 ppt). Snowpack Br_2 fluxes in previous modeling studies are generally on the order of 10^7-10^9 molec cm^{-2} s^{-1} for Br_2 [*Piot and von Glasow*, 2008; *Piot and von Glasow*, 2010; *Toyota et al.*, 2014]. Note that these earlier modeling studies were conceptually set up for polar environments, and not extensively tested with speciated reactive halogen measurements, partially due to the lack of high resolution, speciated measurements of reactive halogens.

4.8. Budget Analysis of Molecular Halogens

In this section, we explore the sources and sinks of molecular halogens for both 15 and 24 March using the modeling scenarios that provided the best agreement with measurements: (i) 15 March: NO_x S2, Br_2 SSmod (Section 4.5) and Cl_2 SSmod (Section 4.6); (ii) 24 March: Br_2 Jscale (Section 4.5) and Cl_2 SSmod (Section 4.6). The mid-day (12:00-14:00 AKST) sources and sinks of molecular halogens are summarized in Table 2. Modeled concentrations of a number of other species, including BrCl, are shown in Figures S8 and S9, with discussion of possible BrCl sources and sinks in the supplementary information (Section S3).

4.8.1. Cl_2 sources and sinks

Heterogeneous recycling pathways contribute to ambient Cl_2, in addition to snowpack emissions, or heterogeneous recycling (R5 and R9). On 24 March, measured

daytime Cl_2 reached 20 ppt, with the $ClONO_{2(g)} + Cl^-_{(aq)}$ reaction on surface snow suggested to contribute to 51% of Cl_2 production at noontime on this day (Table 2). The simulated direct snowpack Cl_2 emission, from condensed-phase reactions (Section 4.7), contributed the remaining 49% of the total Cl_2 production. On 15 March, however, when measured Cl_2 was relatively low (up to 9 ppt in the morning and nearly zero at noontime), the model results suggest that direct snowpack emissions account for 27% of the Cl_2 source, with the rapid $ClONO_{2(g)} + Cl^-_{(aq)}$ reaction on the surface snow contributing the remaining 73% of total Cl_2 production at noontime. On both 15 and 24 March, the multiphase reaction of $ClONO_2$ with surface snow chloride plays a key role in the Cl_2 production, while the role of HOCl in Cl_2 production is suggested to be negligible in the model. On 24 March, up to 18 ppt of HOCl is produced in the model; however, as shown in Figure 4, $ClONO_2$ formation is favored over HOCl for typical NO_x and HO_x levels measured in Utqiaġvik (modeled $ClONO_2$ remained <1 ppt on 15 March but reached 15 ppt on 24 March). In addition, aqueous-phase reactions of HOCl are slower than that of HOBr (Table S5), and the reaction of $HOCl + Br^-_{(aq)}$ is ~100 times faster than HOCl reaction with $Cl^-_{(aq)}$ [*Liu and Margerum,* 2001]. In a previous 1-D modeling study, Toyota et al. [2014] predicted < 2 ppt Cl_2, which clearly is not consistent with the elevated reactive chlorine levels reported during OASIS [*Liao et al.,* 2014] and BROMEX [*Custard et al.,* 2016]. In this work, we found that the multiphase reaction of $ClONO_2$ with snow Cl^- may play a key role in Cl_2 snowpack production and rival

condensed phase Cl_2 production (Table 2); however, this remains untested due to the lack of ambient $ClONO_2$ measurements.

As discussed in Section 4.2, photolysis alone is not sufficient to explain the rapid Cl_2 depletion in the late afternoon. In the model we included the heterogeneous reaction of $Cl_2 + Br^-_{(aq)}$ (R14). On both 15 and 24 March, this heterogeneous reaction accounted for a substantial Cl_2 sink (37% on 15 March (snow only) and 15% on 24 March (13% aerosol, 2% snow)). In comparison, modeling scenarios (not shown) with a lower limit Cl_2 reactive uptake coefficient of 0.004 showed excess Cl_2 at night (> 10 ppt), in contrast to the near zero nocturnal Cl_2 in this work (Figure 1) and previous work [*Custard et al.*, 2016; *Liao et al.*, 2014]. The heterogeneous reaction of $Cl_2 + Br^-_{(aq)}$ has not been included in previous Arctic modeling studies [*Piot and von Glasow*, 2010; *Thomas et al.*, 2011; *Toyota et al.*, 2014], although the bulk reaction between dissolved Cl_2 and bromide in quasi-liquid layers have been considered in these multiphase models. Laboratory studies by Hu et al [1995], showed rapid Cl_2 uptake that could only be explained by the heterogeneous reaction at the surface, rather than in the bulk. The second order reaction rate of $Cl_2 + Br^-_{(aq)}$ inferred from uptake experiments [*Hu et al.*, 1995] is up to a factor of 3.4 faster than the rate coefficient of $Cl_2 + Br^-_{(aq)}$ in bulk solutions [*Liu and Margerum*, 2001]. This is consistent with Cl_2 reactive uptake on bromide-containing ice (233 K) [*Huff and Abbatt*, 2000]. Given the potential impact on the Cl_2 budget, the heterogeneous

removal of Cl_2 by reaction with both snow and aerosol bromide should be included in future modeling studies.

4.8.2. Br_2 sources and sinks

The major modeled Br_2 sources and sinks are summarized in Table 2. On both 15 and 24 March, the modeling results suggest that recycling mechanisms (in both gas-phase and surface snow) play a major role in the production of Br_2. On 15 March, when O_3 was depleted and Br_2 was elevated (nighttime up to 53 ppt), the gas-phase reaction of Br atoms with $BrNO_2$ and $BrONO_2$ (R15 and R16) together are estimated to account for 70% of the total Br_2 production. On 24 March, when O_3 was at background conditions (~30 ppb) and nighttime Br_2 was lower (up to 21 ppt), the BrO self-reaction (R11) and Br + $BrONO_2$ reaction (R16) contribute to 18% and 55%, respectively, of the total Br_2 source. Note that none of these reactions (R11, R15, and R16) are net bromine sources. Multiphase reactions (with both particles and surface snowpack) involving $BrONO_2$ together add another 6% (24 March; 4% on aerosols and 2% on snow) and <1% (15 March) of Br_2 production. Therefore, $BrONO_2$ may play an important role in bromine recycling even under typical Utqiaġvik conditions (previously measured NO_x: 84±159 ppt [*Villena et al.*, 2011]).

The role of HOBr in bromine activation has been highlighted in Arctic modeling studies for decades [*Evans et al.*, 2003; *Fan and Jacob*, 1992]. Due to the lack of direct observations, HOBr was not thoroughly evaluated until recently. Liao et al [2012a] found

that observed HOBr levels were overestimated by a simple steady-state model. In this work, modeled HOBr using the multiphase model (in the best modeling scenario, see Section 4.8) shows reasonable agreement with ambient measurements of HOBr (Figures 5 and S5). Heterogeneous reactions of HOBr on atmospheric particles contributes 8% of the total Br_2 source on 15 March (<1% on snow) and 14% on 24 March, corresponding to 28% (15 March) and 54% (24 March) net Br_2 production, with the remainder from condensed-phase snow emissions (Table 2). Given the simulation uncertainties associated with air-snow interactions and the predicted importance of HOBr heterogeneous reactions, the role of HOBr in snowpack halogen activation warrants further evaluation.

5. Conclusions and Implications

We examined the chemical mechanisms controlling the diurnal patterns in atmospheric molecular chlorine and bromine in the Arctic spring, with evaluation using a detailed suite of measurement data of reactive halogen species. We focused on two case studies, corresponding to observations made near Utqiaġvik, AK: 15 March 2012, when elevated daytime levels of Br_2 (9~20 ppt) were observed, and 24 March 2012, which featured elevated daytime Cl_2 (~20 ppt). Major findings are summarized as follows:

(i) Reactive uptake of Cl_2 on aerosols and the surface snowpack is suggested to play a key role in the loss of boundary layer Cl_2. The reaction, $Cl_2 + Br^-_{(aq)}$, is a net source of reactive bromine as BrCl. Without this reaction, modeled Cl_2 does not decline to near zero at night as observed. Although the bulk reaction of $Cl_2 + Br^-_{(aq)}$ is included in many

multiphase models, laboratory experiments indicate that the rapid Cl_2 uptake is a result of surface reaction rather than bulk [*Hu et al.*, 1995; *Huff and Abbatt*, 2000]. Previously Liao et al [2014] showed that BrCl was correlated with the measurement-derived Cl_2 loss rate, consistent with our finding. It should be noted that BrCl may also be produced from $HOBr/BrONO_2 + Cl^-_{(aq)}$ (R6, R10). Future simultaneous measurements of BrCl with HOBr and Cl_2 are needed to provide further understanding of coupled bromine and chlorine chemistry.

(ii) $BrONO_2$ and $ClONO_2$ may play a key role in reactive halogen chemistry in the Arctic, consistent with other modeling studies [*Evans et al.*, 2003; *Thomas et al.*, 2012]. For typical background NO_x and HO_2 levels at Utqiaġvik, the formation of $BrONO_2$ and $ClONO_2$ is favored over HOBr and HOCl. Our model predicts that $ClONO_2$ and $BrONO_2$ may reach tens of ppt, but the modeled $XONO_2$ is subject to potential uncertainties because the multiphase chemistry remains poorly understood. The gas-phase reaction of Br atoms with $BrONO_2$ and $BrNO_2$ is suggested to lead to the observed elevated levels of Br_2 during daytime when O_3 is depleted (< 10 ppb). Previous isotopic analyses suggest that snowpack NO_x emission is coupled to bromine chemistry by the formation and subsequent multiphase reaction of $BrONO_2$ [*Morin et al.*, 2012; *Morin et al.*, 2008]. Snow interstitial air NO_x levels can be three to more than 10 times higher than in the atmosphere above [Honrath et al., 1999]. This suggests that $ClONO_2$ and $BrONO_2$ may have greater contributions to halogen activation within the snowpack. To our

knowledge, $ClONO_2$ and $BrONO_2$ have not been directly measured in the Arctic boundary layer or snowpack interstitial air. Analytical advances are needed to measure atmospheric $ClONO_2$ and $BrONO_2$ to quantify their roles in atmospheric and snowpack halogen chemistry.

(iii) Snowpack emissions of Br_2 and Cl_2 are parameterized in this work, and the results are compared to a detailed suite of atmospheric halogen measurements [*Custard et al.*, 2016; *Peterson et al.*, 2015], as well as recent Br_2 and Cl_2 flux measurements [*Custard et al.*, 2017]. An improved understanding of physical and chemical processes in the snowpack, the phase state of key reactants, as well as air-snow interactions [*Domine et al.*, 2013] is required to improve predictions of the atmospheric composition in the rapidly changing climate. Laboratory experiments using artificial snow or ice films are also needed to further investigate the photochemical production mechanisms of molecular halogens, with respect to the impacts of nitrate, H_2O_2, and carbonyls on halogen activation in the saline snowpack. Further, application of more advanced emission flux measurement techniques, e.g. eddy covariance, are desired for future measurements of snowpack emissions of molecular halogens during springtime ODEs.

(iv) An inherent limitation of this 0-D emission-based model is its lack of vertical coordinate. The results and implications herein are reflective of the near-surface Arctic boundary layer. Future measurements and 1-D modeling are need to determine the effective mixing heights of reactive halogens; to date, 1-D models remain largely

untested due to the lack of vertically resolved measurements. Speciated reactive halogen measurements (especially BrCl, HOCl, $ClNO_2$, $BrNO_2$, $ClONO_2$, $BrONO_2$) are needed in three dimensions, especially the vertical scale, for model evaluation, particularly to further evaluate the associated multiphase recycling mechanisms.

Acknowledgements

This modeling study was supported by National Science Foundation (PLR1417668 and ARC-1107695). 2012 BROMEX CIMS data are available via the NSF Arctic Data Center (Paul Shepson, 2014. Studies of the Production of Molecular Halogens in Arctic Snowpacks and on Sea Ice Surfaces. urn:node:ARCTIC. urn:uuid:8d98e442-1fc5-4d91-94ca-c4039cbe76be). UMIAQ and Polarfield Services are thanked for Utqiaġvik logistics assistance. NOAA Barrow Observatory data were used to set up the model (https://www.esrl.noaa.gov/gmd/obop/brw/). The authors acknowledge Brian Vasel and Edward J. Dlugokencky (NOAA ESRL Global Monitoring Division) for the meteorological and CH_4 data. Patricia Quinn and Lucia Upchurch (NOAA Pacific Marine Environmental Laboratory) are thanked for particulate inorganic ion data. Detlev Helmig and Jacques Hueber (University of Colorado Boulder) are thanked for the non-methane hydrocarbon data. Peter Peterson and Stephen McNamara (University of Michigan) are thanked for helpful discussions. This paper is submitted in memory of our mentor, colleague, and friend Roland von Glasow (University of East Anglia).

Tables and Figures

Table 1. Modeled daytime average (6:00-20:00 AKST) mole ratios (ppt, pmol mol^{-1}) of NO_x, PAN, HONO, and H_2O_2 for base case model scenarios (Section 3.2) and comparison with previous observations. For 15 March 2012, two NO_x scenarios (NO_x S1 and S2) were tested.

Species (ppt)	Modeled			Previous Arctic Measurements	Reference
	15 Mar (NO_x S1)	15 Mar (NO_x S2)	24 Mar		
NO_x	9	70	19	84±159 (background)	(i)
PAN	177	434	35	220±60 (background)	(ii)
HONO	0.2	0.3	1.4	Mean 0.4~10 (background)	(i)
H_2O_2	2285	2364	2040	300~3500	(iii)

Note: (i) NO_x measurements near Utqiaġvik during March 2009: Custard et al [2015]; HONO and NO_x measurements near Utqiaġvik during March 2009: Villena et al [2011]; (ii) PAN measurements (0-3 km, background conditions) from ARCTAS-A in spring 2008: Liang et al [2011]; (iii) H_2O_2 measurements at Summit, Greenland: Jacobi et al [2002]; and Sigg et al [1992]

Table 2. Mid-day (12:00-14:00 local time) budgets of Cl_2 and Br_2 for the 15 and 24 March cases, both for base case scenarios (Section 4.8). (p) and (s) represent heterogeneous reactions that occur on aerosol particles and surface snow, respectively. Minor pathways (<1%) are not shown.

Species	Pathways	15 Mar (NO_x S2)	24 Mar
Cl_2	**Total source**	**4.1×10^3 molec cm^{-3} s^{-1}**	**4.8×10^5 molec cm^{-3} s^{-1}**
	Snowpack emission	27%	49%
	$ClONO_2+Cl^-_{(aq)}$	73% (s)	51% (s)
	Total sink	**7.1×10^3 molec cm^{-3} s^{-1}**	**5.3×10^5 molec cm^{-3} s^{-1}**
	$Cl_2+h\upsilon$	55%	85%
	$Cl_2+Br^-_{(aq)}$	7% (p), 37% (s)	13% (p), 2% (s)
Br_2	**Total source**	**9.7×10^6 molec cm^{-3} s^{-1}**	**4.5×10^5 molec cm^{-3} s^{-1}**
	Snowpack emission	20%	6%
	BrO+BrO	2%	18%
	$BrONO_2+Br$	19%	55%
	$BrNO_2$/BrONO+Br	51%	1%
	$HOBr+Br^-_{(aq)}$	8% (p)	14% (p)
	$BrONO_2+Br^-_{(aq)}$	<1% (s)	4% (p), 2% (s)
	Total sink	**9.9×10^6 molec cm^{-3} s^{-1}**	**4.5×10^5 molec cm^{-3} s^{-1}**
	$Br_2+h\upsilon$	100%	100%
BrCl	**Total source**	**6.6×10^4 molec cm^{-3} s^{-1}**	**5.6×10^5 molec cm^{-3} s^{-1}**
	BrO+ClO	<1%	11%
	Br_2+Cl	2%	<1%
	$Cl_2+Br^-_{(aq)}$	4% (s)	12% (p), 2% (s)
	$HOBr+Cl^-_{(aq)}$	86% (p)	67% (p), 2% (s)
	$ClONO_2+Br^-$	5% (s)	6% (s)
	Total sink	**7.1×10^4 molec cm^{-3} s^{-1}**	**5.5×10^5 molec cm^{-3} s^{-1}**
	BrCl+hυ	100%	100%

Figure Captions:

Figure 1. Ambient measurements of O_3, Cl_2, ClO, Br_2, BrO, and HOBr mole ratios (1 h averages), as well as solar radiation, on 15 and 24 March 2012 near Utqiaġvik, AK. Error bars represent CIMS measurement uncertainties.

Figure 2. Afternoon Cl_2 loss is investigated through panels (A), (B), and (C) for 15 March, and panels (D), (E), and (F) for 24 March. Panels (A) and (D): measured Cl_2 (30 min average) and solar radiation. Panels (B) and (E): net rate of Cl_2 change calculated from measured Cl_2 (error bar propagated from measurement uncertainty), and Cl_2 loss rate due to photolysis (shading: ±30%). Panels (C) and (F): Cl_2 loss due to heterogeneous reaction ($Cl_2 + Br^-_{(aq)} \rightarrow BrCl + Cl^-_{(aq)}$; k_{het} is given in Eq.S1, γ=0.16 upper limit; measured Cl_2 and aerosol surface area); Cl_2 loss due to dry deposition (dry deposition velocity: 2.8×10^{-5} m s^{-1}; 10 m mixing layer height).

Figure 3. Modeled mid-day (12:00-14:00, AKST) Br_2 / BrO ratios (color-scales) as a function of O_3 and NO_2. The black contours show the calculated Br / BrO ratios (local noon). For each simulation, O_3 and NO_2 were held constant, and the Br_2 / BrO and Br / BrO ratios after three days of spin-up are plotted. All reactive chlorine species were set to zero for these simulations. Circles are mid-day averages of O_3 and NO_2 measured in March-April 2009 during OASIS campaign (background conditions) [*Liao et al.*, 2012a], color-coded by CIMS measured

ambient Br_2 / BrO ratio (same color-scale). Data collected during the entire OASIS campaign were examined, but only data on O_3-depleted days are available for analysis; on high O_3 days there was either town influence or missing data.

Figure 4. (A) Ratio of simulated $ClONO_2$ production rate (P_{ClONO2}) vs simulated HOCl production rate (P_{HOCl}) as a function of NO_2 and HO_2, at 298 and 248 K; (B) same for $BrONO_2$ vs HOBr. Box and error bars show average and standard deviation of NO_2 and HO_2 measured during background conditions in March 2009 near Utqiaġvik, AK [*Villena et al.*, 2011]. The arrows indicate the maximum NO_2 during the same study [*Villena et al.*, 2011].

Figure 5. O_3 and reactive bromine species modeled for 15 March, compared to measurements. Panel (A)-(E) and (F)-(J) are under different NO_x scenarios: NO_x S1 and S2, respectively, as defined in Section 3.2. For both NO_x S1 and S2, three Br_2 snowpack emission scenarios are tested: JScale (emission rate scaled with j_{Br2}), SS (emission rate calculated from steady-state of Br_2), and SS_mod (modified based on SS; difference is shown as shading). Black dots and error bars represent measurements (same as in Figure 1).

Figure 6. Modeled Cl_2 and ClO under different Cl_2 snowpack emission scenarios (Jscale, SS and SSmod, as detailed in Section 3.1) for 24 March. Black dots and error bars represent measurements.

References

Abbatt, J. P. D., et al. (2012), Halogen activation via interactions with environmental ice and snow in the polar lower troposphere and other regions, *Atmos. Chem. Phys.*, *12*(14), 6237-6271, doi:10.5194/acp-12-6237-2012.

Ammann, M., R. A. Cox, J. N. Crowley, M. E. Jenkin, A. Mellouki, M. J. Rossi, J. Troe, and T. J. Wallington (2013), Evaluated kinetic and photochemical data for atmospheric chemistry: Volume VI – heterogeneous reactions with liquid substrates, *Atmos. Chem. Phys.*, *13*(16), 8045-8228, doi:10.5194/acp-13-8045-2013.

Atkinson, R., D. L. Baulch, R. A. Cox, J. N. Crowley, R. F. Hampson, R. G. Hynes, M. E. Jenkin, M. J. Rossi, and J. Troe (2006), Evaluated kinetic and photochemical data for atmospheric chemistry: Volume II - gas phase reactions of organic species, *Atmos. Chem. Phys.*, *6*, 3625-4055.

Barrie, L., J. Bottenheim, R. Schnell, P. Crutzen, and R. Rasmussen (1988), Ozone destruction and photochemical reactions at polar sunrise in the lower Arctic atmosphere, *Nature*(334), 138-141, doi:doi:10.1038/334138a0.

Bartels-Rausch, T., et al. (2014), A review of air–ice chemical and physical interactions (AICI): liquids, quasi-liquids, and solids in snow, *Atmos. Chem. Phys.*, *14*(3), 1587-1633, doi:10.5194/acp-14-1587-2014.

Beckwith, R. C., T. X. Wang, and D. W. Margerum (1996), Equilibrium and Kinetics of Bromine Hydrolysis, *Inorganic Chemistry*, *35*(4), 995-1000, doi:10.1021/ic950909w.

Bloss, W. J., M. Camredon, J. D. Lee, D. E. Heard, J. M. C. Plane, A. Saiz-Lopez, S. J. B. Bauguitte, R. A. Salmon, and A. E. Jones (2010), Coupling of HOx, NOx and halogen chemistry in the antarctic boundary layer, *Atmos. Chem. Phys.*, *10*(21), 10187-10209, doi:10.5194/acp-10-10187-2010.

Burkholder, J. B., S. P. Sander, J. Abbatt, J. R. Barker, R. E. Huie, C. E. Kolb, M. J. Kurylo, V. L. Orkin, D. M. Wilmouth, and P. H. Wine (2015), Chemical Kinetics and Photochemical Data for Use in Atmospheric Studies, Evaluation No. 18, *JPL Publication 10-6, Jet Propulsion Laboratory, Pasadena, http://jpldataeval.jpl.nasa.gov* .

Buys, Z., N. Brough, L. G. Huey, D. J. Tanner, R. von Glasow, and A. E. Jones (2013), High temporal resolution Br2, BrCl and BrO observations in coastal Antarctica, *Atmos. Chem. Phys.*, *13*(3), 1329-1343, doi:10.5194/acp-13-1329-2013.

Caloz, F., F. F. Fenter, and M. J. Rossi (1996), Heterogeneous Kinetics of the Uptake of ClONO2 on NaCl and KBr, *The Journal of Physical Chemistry*, *100*(18), 7494-7501, doi:10.1021/jp953099i.

Calvert, J. G., and S. E. Lindberg (2003), A modeling study of the mechanism of the halogen–ozone–mercury homogeneous reactions in the troposphere during the polar spring, *Atmos. Environ.*, *37*(32), 4467-4481, doi:http://dx.doi.org/10.1016/j.atmosenv.2003.07.001.

Cao, L., H. Sihler, U. Platt, and E. Gutheil (2014), Numerical analysis of the chemical kinetic mechanisms of ozone depletion and halogen release in the polar troposphere, *Atmos. Chem. Phys.*, *14*(7), 3771-3787, doi:10.5194/acp-14-3771-2014.

Custard, K. D., K. A. Pratt, S. Wang, and P. B. Shepson (2016), Constraints on Arctic atmospheric chlorine production through measurements and simulations of Cl2 and ClO, *Environ. Sci. Technol.*, doi:10.1021/acs.est.6b03909.

Custard, K. D., A. R. W. Raso, P. Shepson, R. Staebler, and K. A. Pratt (2017), Production and release of molecular bromine and chlorine from the Arctic coastal snowpack, *ACS Earth & Space Chemistry*, *1*(3), 142, doi:10.1021/acsearthspacechem.7b00014.

Custard, K. D., et al. (2015), The NOx dependence of bromine chemistry in the Arctic atmospheric boundary layer, *Atmos. Chem. Phys.*, *15*(18), 10799-10809, doi:10.5194/acp-15-10799-2015.

Deiber, G., C. George, S. Le Calvé, F. Schweitzer, and P. Mirabel (2004), Uptake study of ClONO2 and BrONO2 by Halide containing droplets, *Atmos. Chem. Phys.*, *4*(5), 1291-1299, doi:10.5194/acp-4-1291-2004.

Domine, F., J. Bock, D. Voisin, and D. J. Donaldson (2013), Can We Model Snow Photochemistry? Problems with the Current Approaches, *The Journal of Physical Chemistry A*, *117*(23), 4733-4749, doi:10.1021/jp3123314.

Domine, F., J.-C. Gallet, J. Bock, and S. Morin (2012), Structure, specific surface area and thermal conductivity of the snowpack around Barrow, Alaska, *J. Geophys. Res-Atmos.*, *117*(D14), n/a-n/a, doi:10.1029/2011JD016647.

Dominé, F., and P. B. Shepson (2002), Air-snow interactions and atmospheric chemistry, *Science*, *297*(5586), 1506-1510.

Erbland, J., W. C. Vicars, J. Savarino, S. Morin, M. M. Frey, D. Frosini, E. Vince, and J. M. F. Martins (2013), Air–snow transfer of nitrate on the East Antarctic Plateau – Part 1: Isotopic evidence for a photolytically driven dynamic equilibrium in summer, *Atmos. Chem. Phys.*, *13*(13), 6403-6419, doi:10.5194/acp-13-6403-2013.

Evans, M., D. J. Jacob, E. Atlas, C. Cantrell, F. Eisele, F. Flocke, A. Fried, R. Mauldin, B. Ridley, and B. Wert (2003), Coupled evolution of BrOx-ClOx-HOx-NOx chemistry during bromine-catalyzed ozone depletion events in the arctic boundary layer, *J. Geophys. Res-Atmos.*, *108*(D4).

Fan, S.-M., and D. J. Jacob (1992), Surface ozone depletion in Arctic spring sustained by bromine reactions on aerosols, *Nature*, *359*(6395), 522-524.

Foster, K. L., R. A. Plastridge, J. W. Bottenheim, P. B. Shepson, B. J. Finlayson-Pitts, and C. W. Spicer (2001), The Role of Br2 and BrCl in Surface Ozone Destruction at Polar Sunrise, *Science*, *291*(5503), 471-474, doi:10.1126/science.291.5503.471.

France, J., H. Reay, M. King, D. Voisin, H. Jacobi, F. Domine, H. Beine, C. Anastasio, A. MacArthur, and J. Lee-Taylor (2012), Hydroxyl radical and NOx production rates, black carbon concentrations and light-absorbing impurities in snow from field

measurements of light penetration and nadir reflectivity of onshore and offshore coastal Alaskan snow, *J. Geophys. Res-Atmos.*, *117*(D5).
Frey, M. M., J. Savarino, S. Morin, J. Erbland, and J. M. F. Martins (2009), Photolysis imprint in the nitrate stable isotope signal in snow and atmosphere of East Antarctica and implications for reactive nitrogen cycling, *Atmos. Chem. Phys.*, *9*(22), 8681-8696, doi:10.5194/acp-9-8681-2009.
Garman, K. E., K. A. Hill, P. Wyss, M. Carlsen, J. R. Zimmerman, B. H. Stirm, T. Q. Carney, R. Santini, and P. B. Shepson (2006), An Airborne and Wind Tunnel Evaluation of a Wind Turbulence Measurement System for Aircraft-Based Flux Measurements, *Journal of Atmospheric and Oceanic Technology*, *23*(12), 1696-1708, doi:doi:10.1175/JTECH1940.1.
Gebel, M. E., and B. J. Finlayson-Pitts (2001), Uptake and Reaction of ClONO2 on NaCl and Synthetic Sea Salt, *The Journal of Physical Chemistry A*, *105*(21), 5178-5187, doi:10.1021/jp0046290.
Grannas, A. M., et al. (2007), An overview of snow photochemistry: evidence, mechanisms and impacts, *Atmos. Chem. Phys.*, *7*(16), 4329-4373, doi:10.5194/acp-7-4329-2007.
Guimbaud, C., et al. (2002), Snowpack processing of acetaldehyde and acetone in the Arctic atmospheric boundary layer, *Atmos. Environ.*, *36*(15–16), 2743-2752, doi:https://doi.org/10.1016/S1352-2310(02)00107-3.
Hausmann, M., and U. Platt (1994), Spectroscopic measurement of bromine oxide and ozone in the high Arctic during Polar Sunrise Experiment 1992, *J. Geophys. Res-Atmos.*, *99*(D12), 25399-25413, doi:10.1029/94JD01314.
Helmig, D., et al. (2012), Ozone dynamics and snow-atmosphere exchanges during ozone depletion events at Barrow, Alaska, *J. Geophys. Res-Atmos.*, *117*(D20), n/a-n/a, doi:10.1029/2012JD017531.
Honrath, R. E., M. C. Peterson, S. Guo, J. E. Dibb, P. B. Shepson, and B. Campbell (1999), Evidence of NOx production within or upon ice particles in the Greenland snowpack, *Geophys. Res. Lett.*, *26*(6), 695-698, doi:10.1029/1999GL900077.
Hu, J. H., Q. Shi, P. Davidovits, D. R. Worsnop, M. S. Zahniser, and C. E. Kolb (1995), Reactive Uptake of Cl2(g) and Br2(g) by Aqueous Surfaces as a Function of Br- and I- Ion Concentration: The Effect of Chemical Reaction at the Interface, *The Journal of Physical Chemistry*, *99*(21), 8768-8776, doi:10.1021/j100021a050.
Huff, A. K., and J. P. D. Abbatt (2000), Gas-Phase Br2 Production in Heterogeneous Reactions of Cl2, HOCl, and BrCl with Halide−Ice Surfaces, *The Journal of Physical Chemistry A*, *104*(31), 7284-7293, doi:10.1021/jp001155w.
Jacob, D. J. (2000), *Atmospheric Chemistry*.
Jacobi, H.-W., M. M. Frey, M. A. Hutterli, R. C. Bales, O. Schrems, N. J. Cullen, K. Steffen, and C. Koehler (2002), Measurements of hydrogen peroxide and formaldehyde exchange between the atmosphere and surface snow at Summit,

Greenland, *Atmos. Environ.*, *36*(15–16), 2619-2628, doi:http://dx.doi.org/10.1016/S1352-2310(02)00106-1.
Kaleschke, L., et al. (2004), Frost flowers on sea ice as a source of sea salt and their influence on tropospheric halogen chemistry, *Geophys. Res. Lett.*, *31*(16), n/a-n/a, doi:10.1029/2004GL020655.
Le Bras, G., and U. Platt (1995), A possible mechanism for combined chlorine and bromine catalyzed destruction of tropospheric ozone in the Arctic, *Geophys. Res. Lett.*, *22*(5), 599-602, doi:10.1029/94GL03334.
Lehrer, E., G. Hönninger, and U. Platt (2004), A one dimensional model study of the mechanism of halogen liberation and vertical transport in the polar troposphere, *Atmos. Chem. Phys.*, *4*(11/12), 2427-2440, doi:10.5194/acp-4-2427-2004.
Liang, Q., et al. (2011), Reactive nitrogen, ozone and ozone production in the Arctic troposphere and the impact of stratosphere-troposphere exchange, *Atmos. Chem. Phys.*, *11*(24), 13181-13199, doi:10.5194/acp-11-13181-2011.
Liao, J., L. Huey, D. Tanner, F. Flocke, J. Orlando, J. Neuman, J. Nowak, A. Weinheimer, S. Hall, and J. Smith (2012a), Observations of inorganic bromine (HOBr, BrO, and Br2) speciation at Barrow, Alaska, in spring 2009, *J. Geophys. Res-Atmos.*, *117*(D6).
Liao, J., et al. (2014), High levels of molecular chlorine in the Arctic atmosphere, *Nature Geosci*, *7*(2), 91-94, doi:10.1038/ngeo2046.
Liao, J., et al. (2012b), Observations of inorganic bromine (HOBr, BrO, and Br_2) speciation at Barrow, AK, in spring 2009, *J. Geophys. Res.*, *117*(D00R16), doi:10.1029/2011JD016641.
Liao, J., H. Sihler, L. Huey, J. Neuman, D. Tanner, U. Friess, U. Platt, F. Flocke, J. Orlando, and P. Shepson (2011), A comparison of Arctic BrO measurements by chemical ionization mass spectrometry and long path-differential optical absorption spectroscopy, *J. Geophys. Res-Atmos.*, *116*(D1).
Liu, Q., and D. W. Margerum (2001), Equilibrium and Kinetics of Bromine Chloride Hydrolysis, *Environ. Sci. Technol.*, *35*(6), 1127-1133, doi:10.1021/es001380r.
Mahajan, A. S., et al. (2010), Evidence of reactive iodine chemistry in the Arctic boundary layer, *J. Geophys. Res-Atmos.*, *115*(D20), n/a-n/a, doi:10.1029/2009JD013665.
Martinez, M., T. Arnold, and D. Perner (1999), The role of bromine and chlorine chemistry for arctic ozone depletion events in Ny-Ålesund and comparison with model calculations, *Annales Geophysicae*, *17*(7), 941-956, doi:10.1007/s00585-999-0941-4.
McConnell, J. C., G. S. Henderson, L. Barrie, J. Bottenheim, H. Niki, C. H. Langford, and E. M. J. Templeton (1992), Photochemical bromine production implicated in Arctic boundary-layer ozone depletion, *Nature*, *355*(6356), 150-152.
Michalowski, B. A., J. S. Francisco, S.-M. Li, L. A. Barrie, J. W. Bottenheim, and P. B. Shepson (2000), A computer model study of multiphase chemistry in the Arctic

boundary layer during polar sunrise, *J. Geophys. Res-Atmos.*, *105*(D12), 15131-15145, doi:10.1029/2000JD900004.

Moore, C. W., D. Obrist, A. Steffen, R. M. Staebler, T. A. Douglas, A. Richter, and S. V. Nghiem (2014), Convective forcing of mercury and ozone in the Arctic boundary layer induced by leads in sea ice, *Nature*, *506*(7486), 81-84, doi:10.1038/nature12924.

Morin, S., J. Erbland, J. Savarino, F. Domine, J. Bock, U. Friess, H. W. Jacobi, H. Sihler, and J. M. F. Martins (2012), An isotopic view on the connection between photolytic emissions of NOx from the Arctic snowpack and its oxidation by reactive halogens, *J. Geophys. Res-Atmos.*, *117*(D14), n/a-n/a, doi:10.1029/2011JD016618.

Morin, S., J. Savarino, M. M. Frey, N. Yan, S. Bekki, J. W. Bottenheim, and J. M. F. Martins (2008), Tracing the Origin and Fate of NOx in the Arctic Atmosphere Using Stable Isotopes in Nitrate, *Science*, *322*(5902), 730-732, doi:10.1126/science.1161910.

Neuman, J. A., et al. (2010a), Bromine measurements in ozone depleted air over the Arctic Ocean, *Atmos. Chem. Phys.*, *10*(14), 6503-6514, doi:10.5194/acp-10-6503-2010.

Neuman, J. A., et al. (2010b), Bromine measurements in ozone depleted air over the Arctic Ocean, *Atmos. Chem. Phys.*, *10*, 6503-6514.

Nghiem, S. V., et al. (2013), Studying Bromine, Ozone, and Mercury Chemistry in the Arctic, *Eos, Transactions American Geophysical Union*, *94*(33), 289-291, doi:10.1002/2013EO330002.

Orlando, J. J., and J. B. Burkholder (2000), Identification of BrONO as the Major Product in the Gas-Phase Reaction of Br with NO2, *The Journal of Physical Chemistry A*, *104*(10), 2048-2053, doi:10.1021/jp993713g.

Oum, K. W., M. J. Lakin, and B. J. Finlayson-Pitts (1998), Bromine activation in the troposphere by the dark reaction of O3 with seawater ice, *Geophys. Res. Lett.*, *25*(21), 3923-3926, doi:10.1029/1998GL900078.

Peterson, P. K., W. R. Simpson, K. A. Pratt, P. B. Shepson, U. Frieß, J. Zielcke, U. Platt, S. J. Walsh, and S. V. Nghiem (2015), Dependence of the vertical distribution of bromine monoxide in the lower troposphere on meteorological factors such as wind speed and stability, *Atmos. Chem. Phys.*, *15*(4), 2119-2137, doi:10.5194/acp-15-2119-2015.

Piot, M., and R. von Glasow (2008), The potential importance of frost flowers, recycling on snow, and open leads for ozone depletion events, *Atmos. Chem. Phys.*, *8*(9), 2437-2467.

Piot, M., and R. von Glasow (2010), Modelling the multiphase near-surface chemistry related to ozone depletions in polar spring, *J. Atmos. Chem.*, *64*(2), 77-105, doi:10.1007/s10874-010-9170-1.

Platt, U., and C. Janssen (1995), Observation and role of the free radicals NO 3, ClO, BrO and IO in the troposphere, *Faraday Discussions*, *100*, 175-198.
Pöschl, U., Y. Rudich, and M. Ammann (2007), Kinetic model framework for aerosol and cloud surface chemistry and gas-particle interactions – Part 1: General equations, parameters, and terminology, *Atmos. Chem. Phys.*, *7*(23), 5989-6023, doi:10.5194/acp-7-5989-2007.
Pratt, K. A., et al. (2013), Photochemical production of molecular bromine in Arctic surface snowpacks, *Nature Geosci*, *6*(5), 351-356, doi:10.1038/ngeo1779.
Quinn, P. K., T. L. Miller, T. S. Bates, J. A. Ogren, E. Andrews, and G. E. Shaw (2002), A 3-year record of simultaneously measured aerosol chemical and optical properties at Barrow, Alaska, *J. Geophys. Res-Atmos.*, *107*(D11), AAC 8-1-AAC 8-15, doi:10.1029/2001JD001248.
Saiz-Lopez, A., A. S. Mahajan, R. A. Salmon, S. J.-B. Bauguitte, A. E. Jones, H. K. Roscoe, and J. M. C. Plane (2007), Boundary Layer Halogens in Coastal Antarctica, *Science*, *317*(5836), 348-351, doi:10.1126/science.1141408.
Saiz-Lopez, A., J. Plane, A. Mahajan, P. Anderson, S. Bauguitte, A. Jones, H. Roscoe, R. Salmon, W. Bloss, and J. Lee (2008), On the vertical distribution of boundary layer halogens over coastal Antarctica: implications for O3, HOx, NOx and the Hg lifetime, *Atmos. Chem. Phys*, *8*(4), 887-900.
Sander, R. (2015), Compilation of Henry's law constants (version 4.0) for water as solvent, *Atmos. Chem. Phys.*, *15*(8), 4399-4981, doi:10.5194/acp-15-4399-2015.
Sander, R., and J. Bottenheim (2012), A compilation of tropospheric measurements of gas-phase and aerosol chemistry in polar regions, *Earth Syst. Sci. Data*, *4*(1), 215-282, doi:10.5194/essd-4-215-2012.
Sander, R., R. Vogt, G. W. Harris, and P. J. Crutzen (1997), Modelling the chemistry of ozone, halogen compounds, and hydrocarbons in the arctic troposphere during spring, *Tellus B*, *49*(5), 522-532, doi:10.1034/j.1600-0889.49.issue5.8.x.
Savarino, J., S. Morin, J. Erbland, F. Grannec, M. D. Patey, W. Vicars, B. Alexander, and E. P. Achterberg (2013), *Proc. Nat. Acad. Sci.*, *110*, 17668.
Shepson, P. B., A. P. Sirju, J. R. Hopper, L. A. Barrie, V. Young, H. Niki, and H. Dryfhout (1996), Sources and sinks of carbonyl compounds in the Arctic Ocean boundary layer: Polar ice floe experiment, *J. Geophys. Res-Atmos.*, *101*(D15), 21081-21089, doi:10.1029/96JD02032.
Sigg, A., T. Staffelbach, and A. Neftel (1992), Gas phase measurements of hydrogen peroxide in Greenland and their meaning for the interpretation of H2O2 records in ice cores, *J. Atmos. Chem.*, *14*(1-4), 223-232, doi:10.1007/BF00115235.
Simpson, W. R., S. S. Brown, A. Saiz-Lopez, J. A. Thornton, and R. v. Glasow (2015), Tropospheric Halogen Chemistry: Sources, Cycling, and Impacts, *Chemical Reviews*, doi:10.1021/cr5006638.

Simpson, W. R., et al. (2007), Halogens and their role in polar boundary-layer ozone depletion, *Atmos. Chem. Phys.*, *7*(16), 4375-4418, doi:10.5194/acp-7-4375-2007.
Spicer, C. W., R. A. Plastridge, K. L. Foster, B. J. Finlayson-Pitts, J. W. Bottenheim, A. M. Grannas, and P. B. Shepson (2002), Molecular halogens before and during ozone depletion events in the Arctic at polar sunrise: concentrations and sources, *Atmos. Environ.*, *36*(15–16), 2721-2731, doi:http://dx.doi.org/10.1016/S1352-2310(02)00125-5.
Steffen, A., J. Bottenheim, A. Cole, T. A. Douglas, R. Ebinghaus, U. Friess, S. Netcheva, S. Nghiem, H. Sihler, and R. Staebler (2013), Atmospheric mercury over sea ice during the OASIS-2009 campaign, *Atmos. Chem. Phys.*, *13*(14), 7007-7021, doi:10.5194/acp-13-7007-2013.
Tackett, P. J., A. E. Cavender, A. D. Keil, P. B. Shepson, J. W. Bottenheim, S. Morin, J. Deary, A. Steffen, and C. Doerge (2007), A study of the vertical scale of halogen chemistry in the Arctic troposphere during Polar Sunrise at Barrow, Alaska, *J. Geophys. Res-Atmos.*, *112*(D7), n/a-n/a, doi:10.1029/2006JD007785.
Tang, T., and J. C. McConnell (1996), Autocatalytic release of bromine from Arctic snow pack during polar sunrise, *Geophys. Res. Lett.*, *23*(19), 2633-2636, doi:10.1029/96GL02572.
Thomas, J. L., J. E. Dibb, L. G. Huey, J. Liao, D. Tanner, B. Lefer, R. von Glasow, and J. Stutz (2012), Modeling chemistry in and above snow at Summit, Greenland – Part 2: Impact of snowpack chemistry on the oxidation capacity of the boundary layer, *Atmos. Chem. Phys.*, *12*(14), 6537-6554, doi:10.5194/acp-12-6537-2012.
Thomas, J. L., J. Stutz, B. Lefer, L. G. Huey, K. Toyota, J. E. Dibb, and R. von Glasow (2011), Modeling chemistry in and above snow at Summit, Greenland – Part 1: Model description and results, *Atmos. Chem. Phys.*, *11*(10), 4899-4914, doi:10.5194/acp-11-4899-2011.
Thompson, C. R., et al. (2015), Interactions of bromine, chlorine, and iodine photochemistry during ozone depletions in Barrow, Alaska, *Atmos. Chem. Phys.*, *15*(16), 9651-9679, doi:10.5194/acp-15-9651-2015.
Timonen, R. S., L. T. Chu, M.-T. Leu, and L. F. Keyser (1994), Heterogeneous reaction of ClONO2(g) + NaCl(s) .fwdarw. Cl2(g) + NaNO3(s), *The Journal of Physical Chemistry*, *98*(38), 9509-9517, doi:10.1021/j100089a025.
Toyota, K., J. C. McConnell, R. M. Staebler, and A. P. Dastoor (2014), Air–snowpack exchange of bromine, ozone and mercury in the springtime Arctic simulated by the 1-D model PHANTAS – Part 1: In-snow bromine activation and its impact on ozone, *Atmos. Chem. Phys.*, *14*(8), 4101-4133, doi:10.5194/acp-14-4101-2014.
Traversi, R., et al. (2014), Insights on nitrate sources at Dome C (East Antarctic Plateau) from multi-year aerosol and snow records, *2014*, doi:10.3402/tellusb.v66.22550.

Villena, G., et al. (2011), Nitrous acid (HONO) during polar spring in Barrow, Alaska: A net source of OH radicals?, *J. Geophys. Res-Atmos.*, *116*(D14), n/a-n/a, doi:10.1029/2011JD016643.

Wang, S., et al. (2015), Active and widespread halogen chemistry in the tropical and subtropical free troposphere, *Proc. Natl. Acad. Sci. U.S.A.*, *112*(30), 9281-9286, doi:10.1073/pnas.1505142112.

Wang, T. X., and D. W. Margerum (1994), Kinetics of Reversible Chlorine Hydrolysis: Temperature Dependence and General-Acid/Base-Assisted Mechanisms, *Inorganic Chemistry*, *33*(6), 1050-1055, doi:10.1021/ic00084a014.

Wesely, M. L. (1989), Parameterization of surface resistances to gaseous dry deposition in regional-scale numerical models, *Atmospheric Environment (1967)*, *23*(6), 1293-1304, doi:http://dx.doi.org/10.1016/0004-6981(89)90153-4.

Wiedensohler, A., et al. (2012), Mobility particle size spectrometers: harmonization of technical standards and data structure to facilitate high quality long-term observations of atmospheric particle number size distributions, *Atmos. Meas. Tech.*, *5*(3), 657-685, doi:10.5194/amt-5-657-2012.

Wren, S. N., D. J. Donaldson, and J. P. D. Abbatt (2013), Photochemical chlorine and bromine activation from artificial saline snow, *Atmos. Chem. Phys.*, *13*(19), 9789-9800, doi:10.5194/acp-13-9789-2013.

Xie, Z. Q., R. Sander, U. Pöschl, and F. Slemr (2008), Simulation of atmospheric mercury depletion events (AMDEs) during polar springtime using the MECCA box model, *Atmos. Chem. Phys.*, *8*(23), 7165-7180, doi:10.5194/acp-8-7165-2008.

Zeng, T., Y. Wang, K. Chance, N. Blake, D. Blake, and B. Ridley (2006), Halogen-driven low-altitude O3 and hydrocarbon losses in spring at northern high latitudes, *J. Geophys. Res-Atmos.*, *111*(D17), n/a-n/a, doi:10.1029/2005JD006706.

Zhao, T. L., S. L. Gong, J. W. Bottenheim, J. C. McConnell, R. Sander, L. Kaleschke, A. Richter, A. Kerkweg, K. Toyota, and L. A. Barrie (2008), A three-dimensional model study on the production of BrO and Arctic boundary layer ozone depletion, *J. Geophys. Res-Atmos.*, *113*(D24), n/a-n/a, doi:10.1029/2008JD010631.

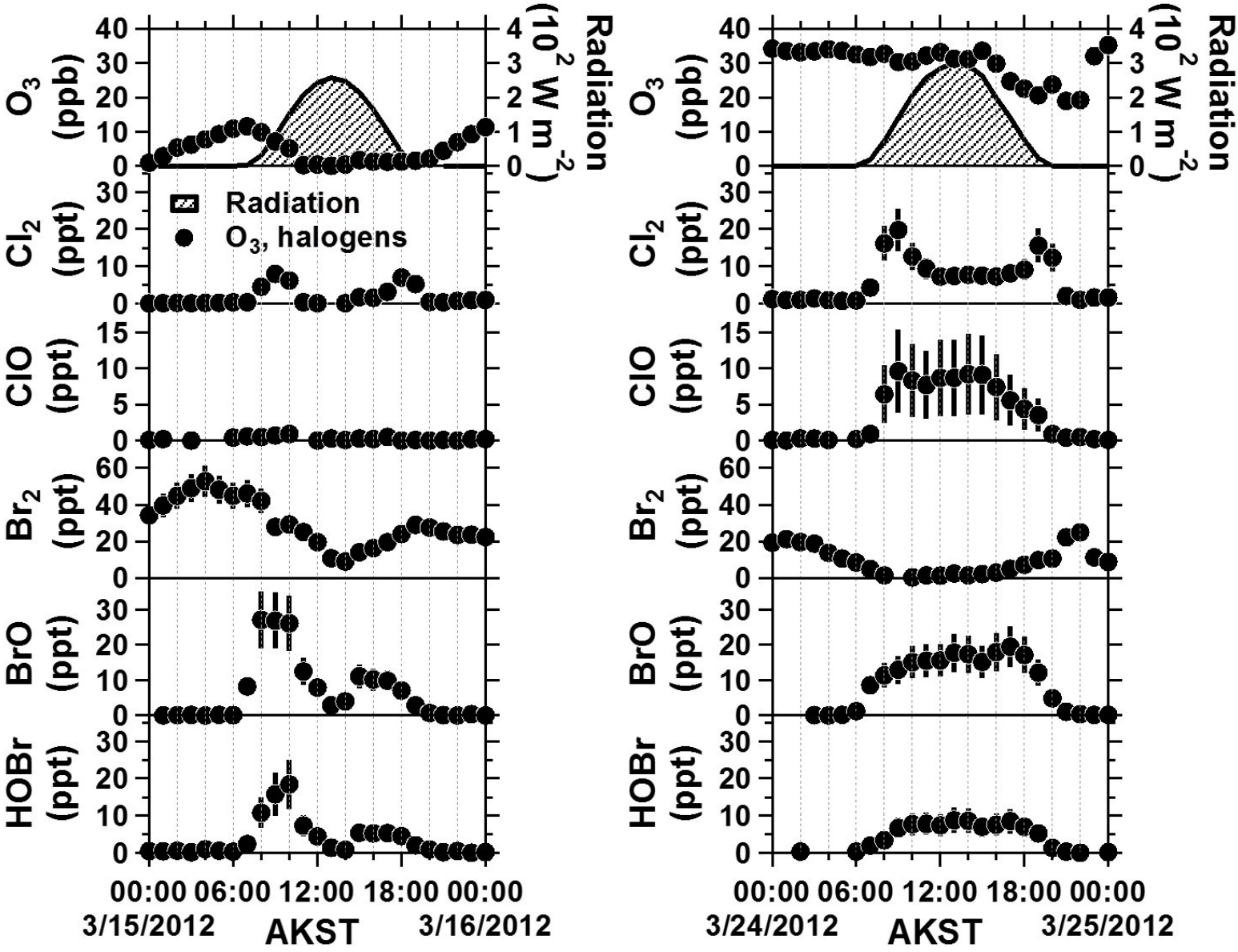

2017JD027175-f01-z-.jpg

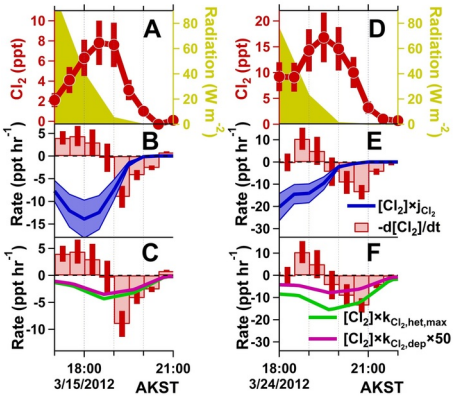

2017JD027175-f02-z-.jpg

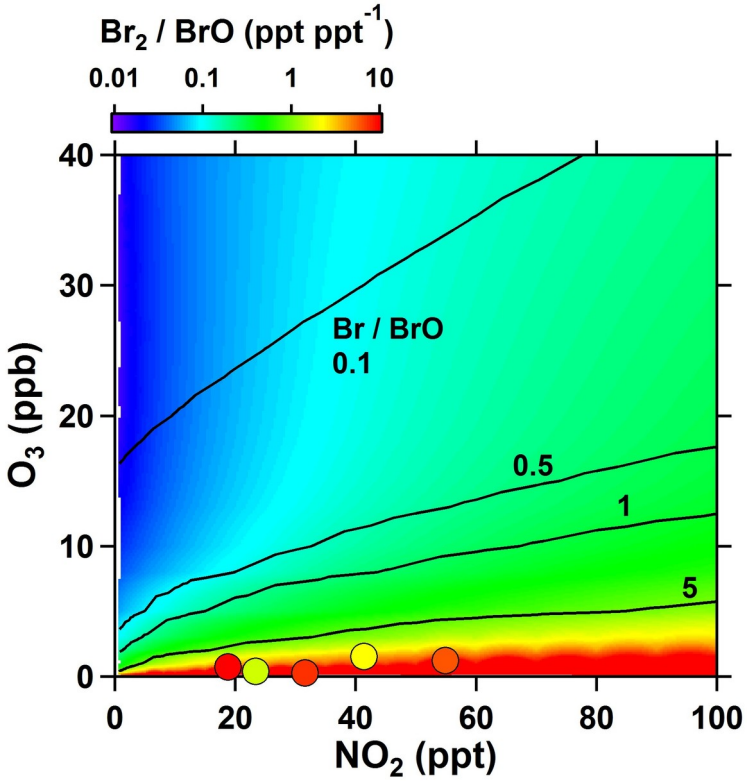

2017JD027175-f03-z-.jpg

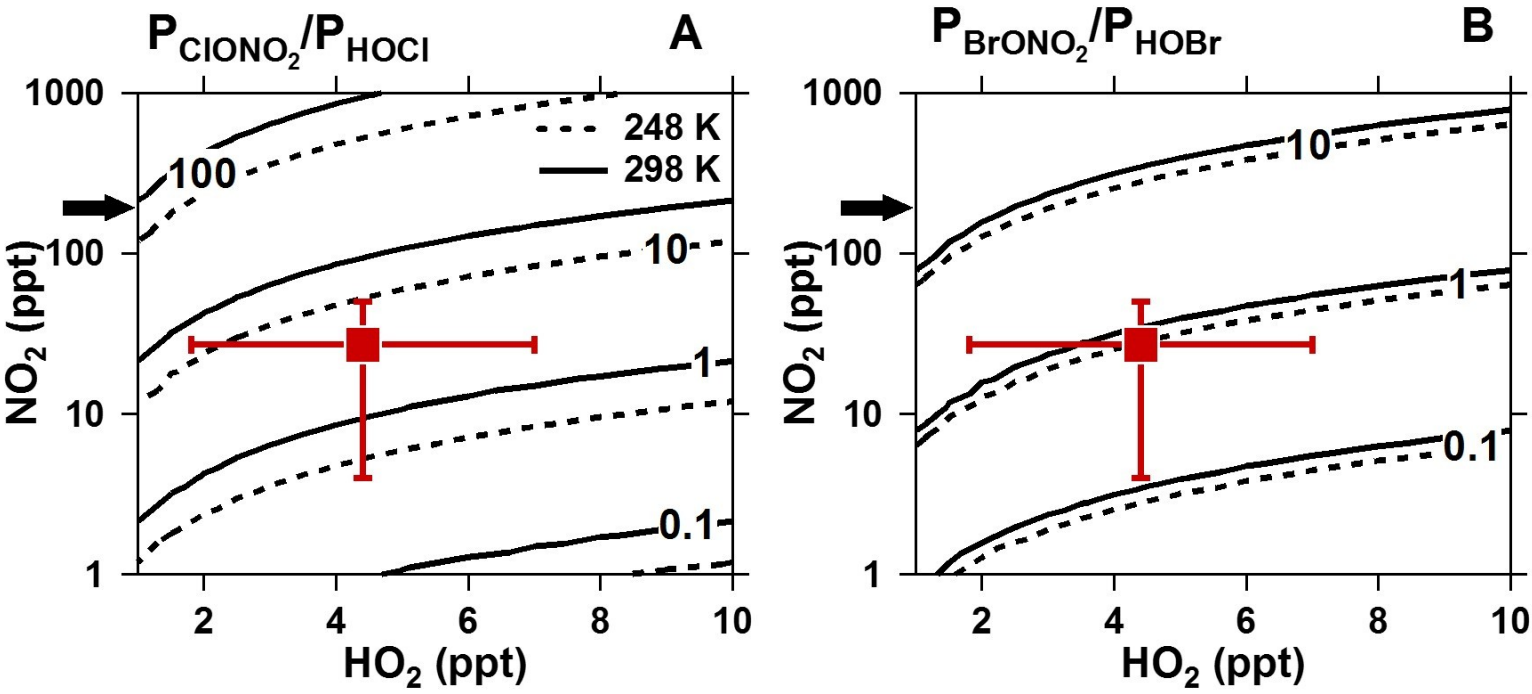

2017JD027175-f04-z-.jpg

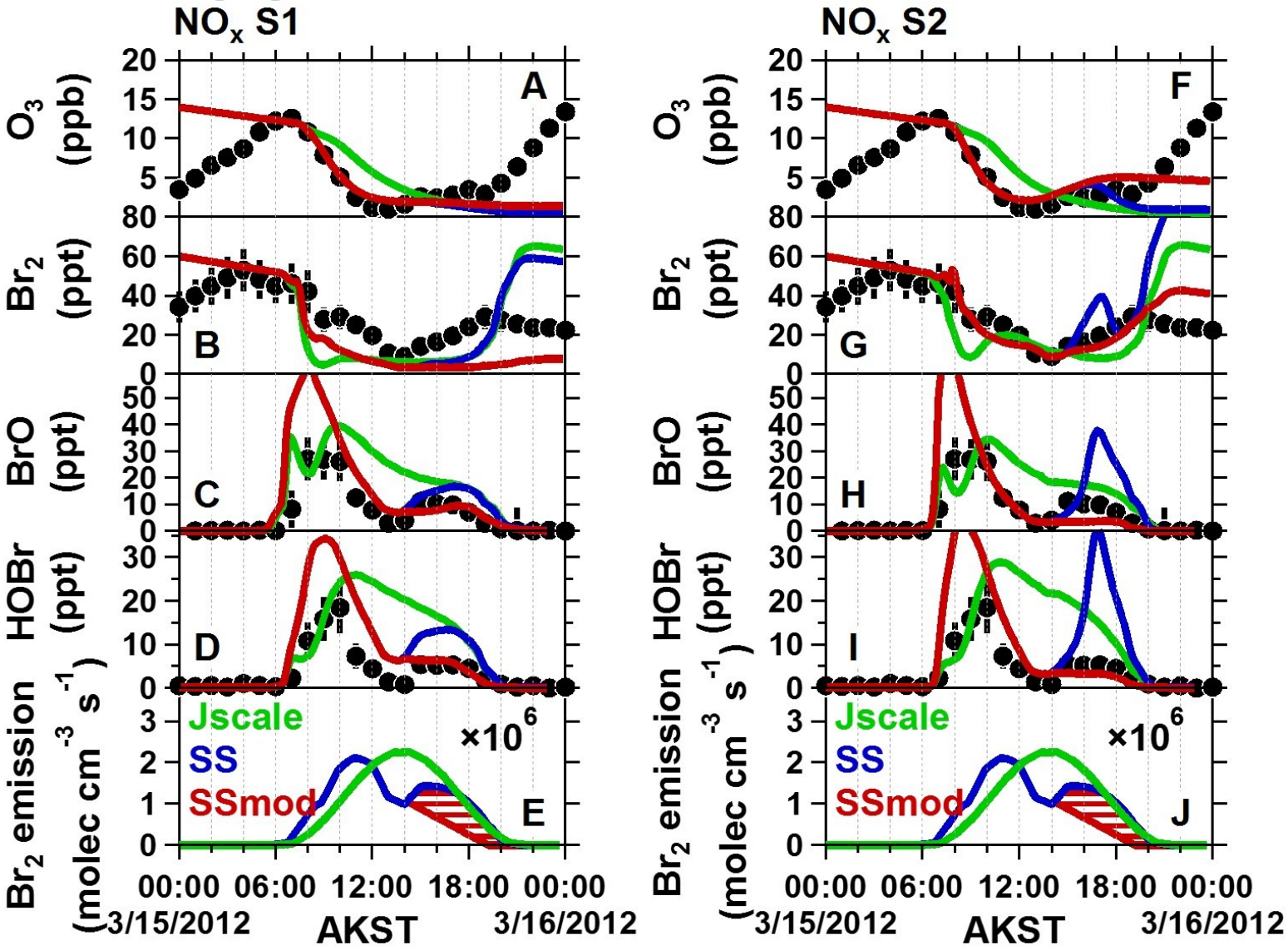

2017JD027175-f05-z-.jpg

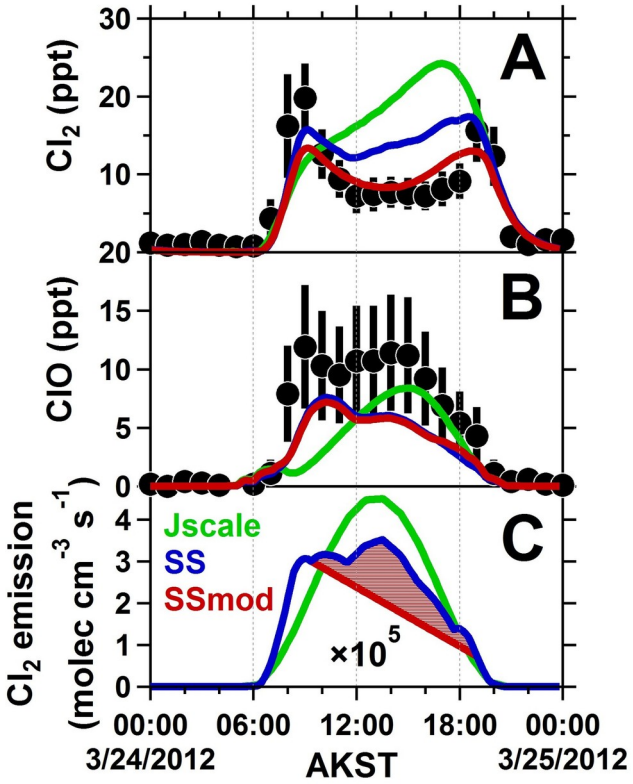

2017JD027175-f06-z-.jpg